Petroleum Science 23 (2026) 4595–4620

Contents lists available at ScienceDirect

Petroleum Science

journal homepage: www.keaipublishing.com/en/journals/petroleum-science

Original Paper

Semi-supervised-learning-based AVO-preserved pre-stack seismic data resolution enhancement

Shu-Liang Wu [a,b], Yi-Ming Jiang [c], Jiang Liu [c], Jian Li [c], De-Wen Qin [c], Jian-Hua Geng [a,b,*]

[a] *Shanghai Key Laboratory of Submarine Resources, Tongji University, Shanghai, 200092, China*
[b] *School of Ocean and Earth Science, Tongji University, Shanghai, 200092, China*
[c] *China National Offshore Oil Corporation Limited Shanghai Branch, Shanghai, 200050, China*

A R T I C L E I N F O

Article history:
Received 30 November 2025
Received in revised form
30 January 2026
Accepted 17 March 2026
Available online 20 March 2026

Edited by Meng-Jiao Zhou

Keywords:
High-resolution
Seismic data processing
Deep learning
Pre-stack data

A B S T R A C T

High-resolution pre-stack seismic data are essential for exploring complex and thin-layered reservoirs, and can enhance the reliability of resource evaluation. However, traditional pre-stack seismic data resolution enhancement methods are single-trace processing unable to preserve the amplitude-versus-offset (AVO) relationships, thus compromising the accuracy of subsequent inversion and interpretation. To address the limitation, a novel semi-supervised learning framework is proposed, enhancing the resolution of pre-stack seismic data and preserving AVO relationships of resolution-enhanced seismic data. The proposed approach integrates physical models with well-log data to train neural networks within a hybrid data- and model-driven framework. The labelled dataset, constructed from well-log data and corresponding amplitude-versus-angle (AVA) gathers, eliminates the assumptions inherent in traditional single-trace reflection coefficient inversion methods. Meanwhile, the physics-guided component utilizes unlabeled seismic data to train neural networks, improving the generalizability of the method. Importantly, this approach preserves AVO relationships during resolution enhancement by leveraging well-log data and the Zoeppritz equation that are essential for elastic parameters inversion. Experiments on both two-dimensional synthetic data and a three-dimensional field data demonstrate that the proposed method can stably extend the frequency bandwidth by 40%, proving its feasibility and effectiveness of the proposed approach.

1. Introduction

High-resolution seismic data significantly enhance the accuracy and efficiency of exploring complex and hidden oil and gas reservoirs, thereby increasing the reliability of resource evaluation (Yilmaz, 2001). Pre-stack amplitude-versus-offset (AVO) gathers that contain AVO relationships, are crucial for subsequent elastic parameter inversion (Aki and Richards, 1980; Rutherford and Williams, 1989; Castagna et al., 1998). However, seismic data resolution is limited by factors such as the bandwidth of seismic wavelets, inelastic effects in underground media, and ambient noise. Deconvolution (Robinson, 1957; Sacchi, 1997; Chen et al., 2022) methods, inverse Q filtering (Hale, 1981; Hu et al., 2013; Wang et al., 2018) methods, and time-frequency analysis (Huang et al., 1998; Daubechies et al., 2011; Liu and Fomel, 2013) methods can enhance the resolution of seismic data, while their performances are often limited by their reliance on various inherent assumptions, such as the minimum phase of the wavelet, white noise reflection coefficients, a constant and frequency-independent Q. Furthermore, pre-stack AVO gathers consist of multi-trace data that contain AVO relationships, which are essential for subsequent elastic parameter inversion. Due to the wavelet tuning effect, the AVO relationships of pre-stack seismic data could change when the bandwidth is broadened. However, aforementioned traditional methods often fail to preserve true AVO relationships during the single-trace resolution enhancement of pre-stack seismic data. The limitation can adversely affect the accuracy of inversion results and reduce the reliability of the interpretation. Furthermore, traditional methods do not incorporate well-log data into the resolution enhancement process. Well-log data can provide the valuable prior information regarding the subsurface model, so they are highly beneficial for improving

* Corresponding author.
E-mail address: jhgeng@tongji.edu.cn (J.-H. Geng).

Peer review under the responsibility of China University of Petroleum (Beijing).

https://doi.org/10.1016/j.petsci.2026.03.040

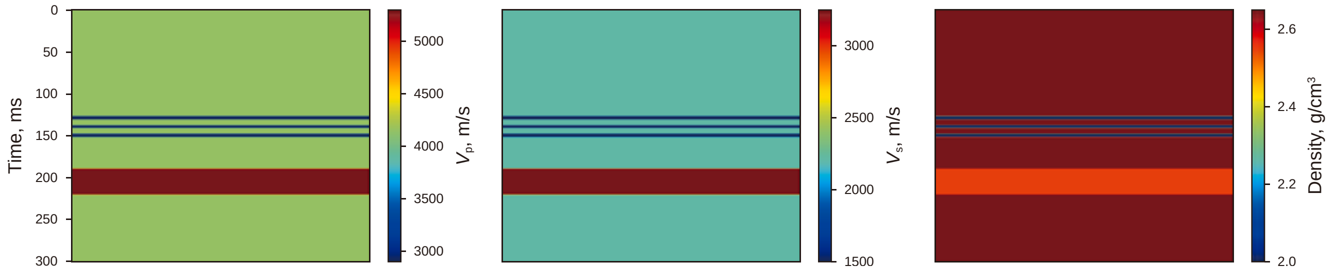

Fig. 1. The elastic model with three thin layers and a thick layer.

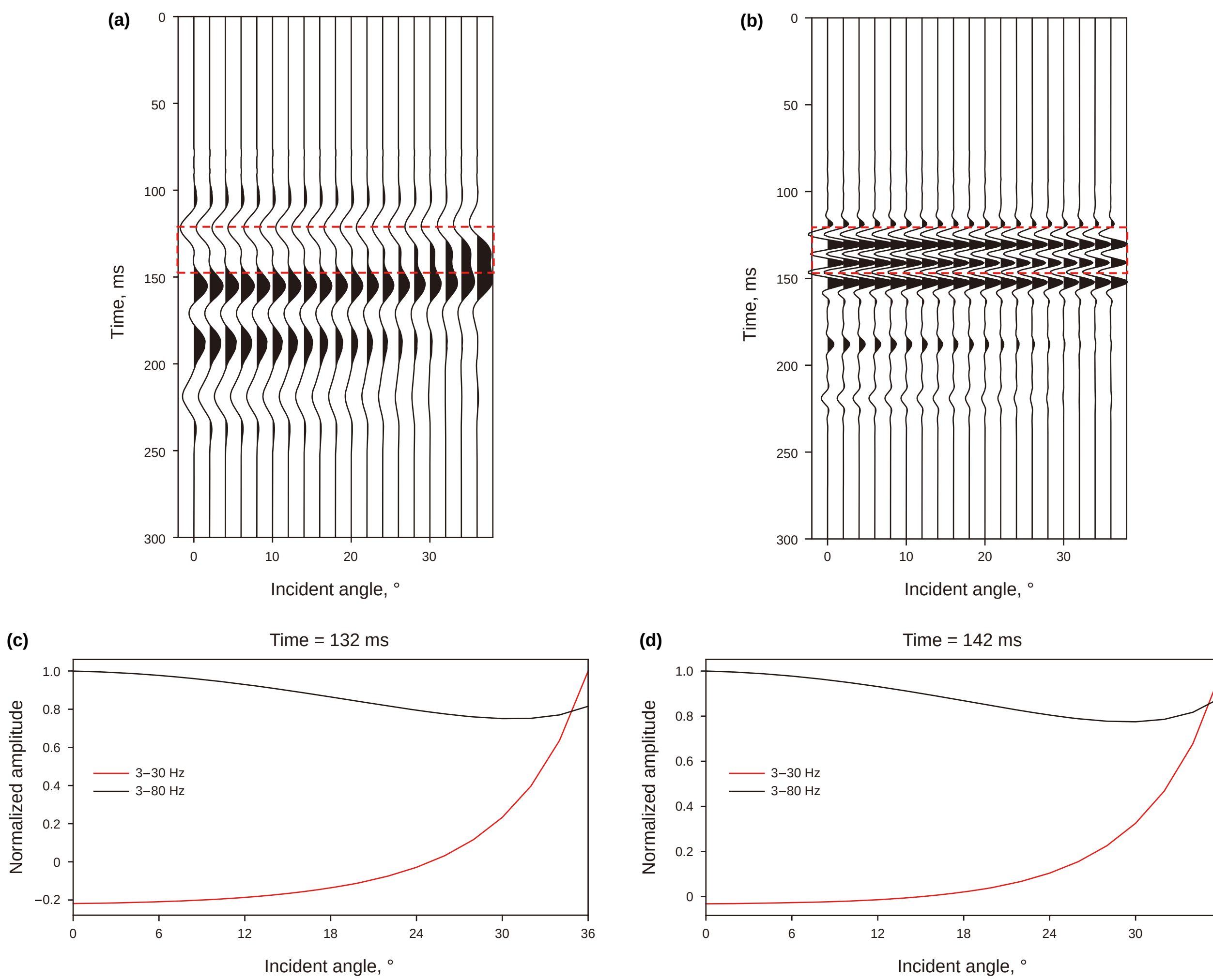

Fig. 2. (**a**), (**b**) Simulated AVA gathers, generated using wavelets with frequency bandwidths of 3–30 Hz and 3–80 Hz, respectively; and (**c**), (**d**) their corresponding AVO relationships at various times.

seismic data resolution. Theoretically, the integration of well-log data within resolution enhancement methods can effectively mitigate the tuning effect and preserve true AVO relationships to some extent.

In recent years, deep learning methods have made significant advancements, with applications in enhancing seismic data resolution. Researchers have utilized deep neural networks in supervised learning frameworks to invert reflection coefficients using well-log data, thereby enhancing seismic data resolution (Kim and Nakata, 2018; Choi et al., 2021; Gao et al., 2022; Guo et al., 2023). Other studies have trained neural networks to map low- and high-frequency data, thereby broadening the frequency band of seismic data (Bevc et al., 2019; Chen et al., 2021, 2023; Cheng et al., 2022; Li et al., 2022; Gao et al., 2023; Liu et al., 2023; Zhang et al., 2024; Lin et al., 2024). However, these supervised methods require large labelled datasets for training. Some approaches generating labels using conventional resolution enhancement methods may inherit their limitations, such as inability to preserve AVO relationships. Others construct high-resolution labels from well-log data, so that they can preserve

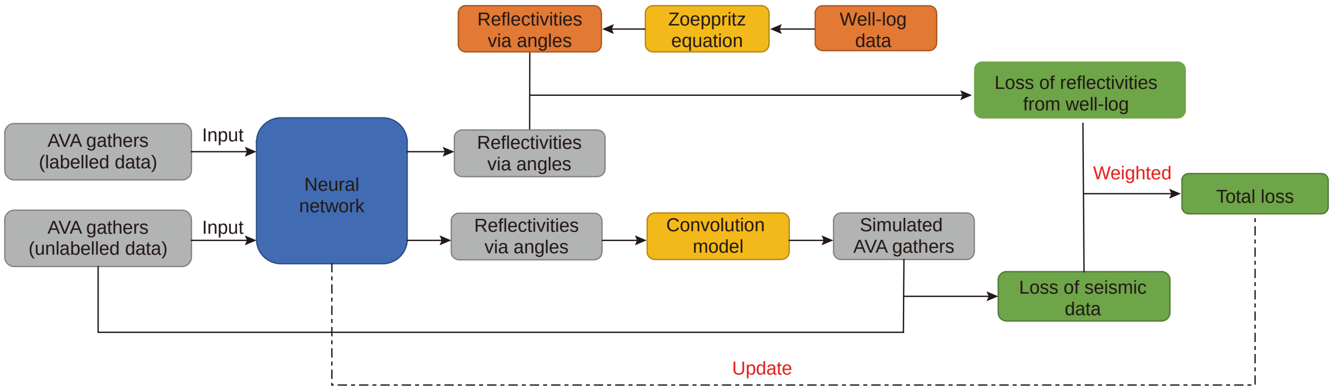

Fig. 3. The framework of the semi-supervised method for resolution enhancement.

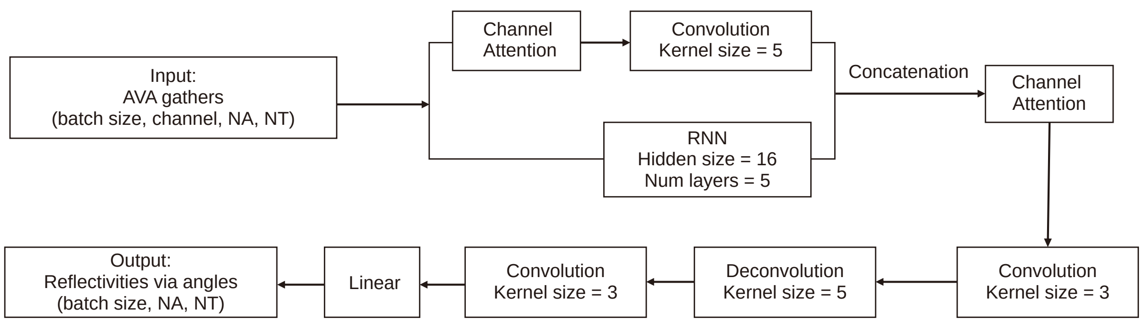

Fig. 4. The structure of neural networks. Channel refers to the number of consecutive AVA gathers; NA refers to the number of angles; NT refers to the number of time samples.

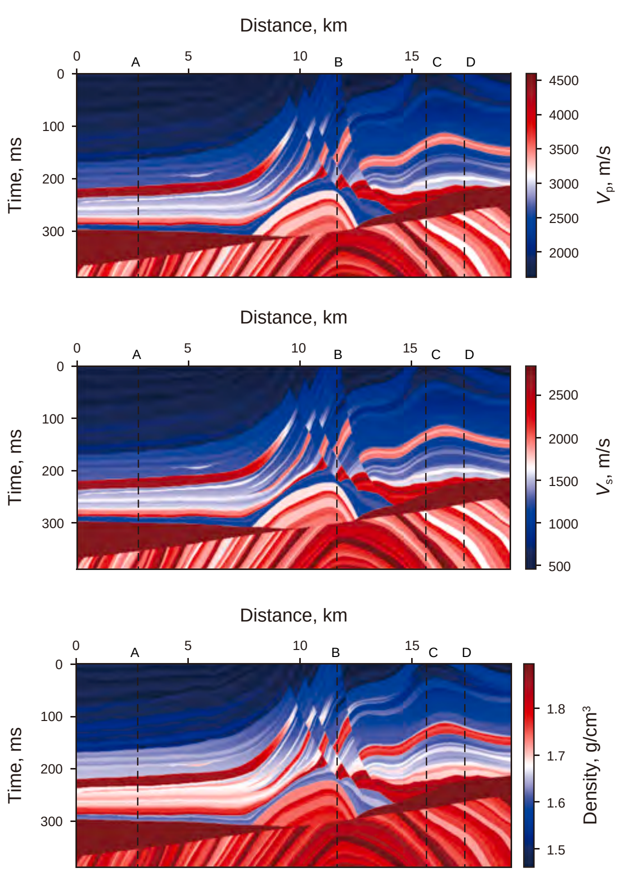

Fig. 5. True elastic model. Black dashed lines denote well locations.

AVO relationships during the resolution enhancement of pre-stack seismic data. Nevertheless, the sparsity of well logs due to high drilling costs limits the generalizability of these methods.

To alleviate the reliance on large labelled datasets, some researchers have proposed training neural networks within semi-supervised and unsupervised learning frameworks. Luo et al. (2023) utilized a closed-loop network to achieve attenuation compensation and Q estimation of post-stack seismic data via semi-supervised learning and Wang et al. (2024) extended this architecture to seismic acoustic impedance estimation. However, these closed-loop network methods do not incorporate physical models. In contrast, Wu et al. (2024), Ge et al. (2024) and Liu et al. (2025) have incorporated physical models into neural networks under semi-supervised learning framework to achieve pre-stack and post-stack seismic inversion. Zhao et al. (2025) have proposed an unsupervised learning deconvolution method for post-stack seismic data by incorporating the Robinson convolution model. However, existing deep learning resolution enhancement methods still lack specialized approaches explicitly targeting pre-stack seismic data. Consequently, these approaches generally fail to preserve true AVO relationships during resolution enhancement.

To address the challenges posed by limited well-log data, enhance the generalizability of neural network-based resolution enhancement methods, and preserve true AVO relationships during resolution enhancement, we propose an AVO-preserved pre-stack seismic data resolution enhancement method under a semi-supervised deep learning framework. Our method employs neural networks to establish a mapping relationship between pre-stack seismic data and subsurface amplitude-versus-angle (AVA) reflection coefficients and requires only a small amount of well-log data to train neural networks. To ensure horizontal consistency, multiple consecutive AVA gathers are input into the neural

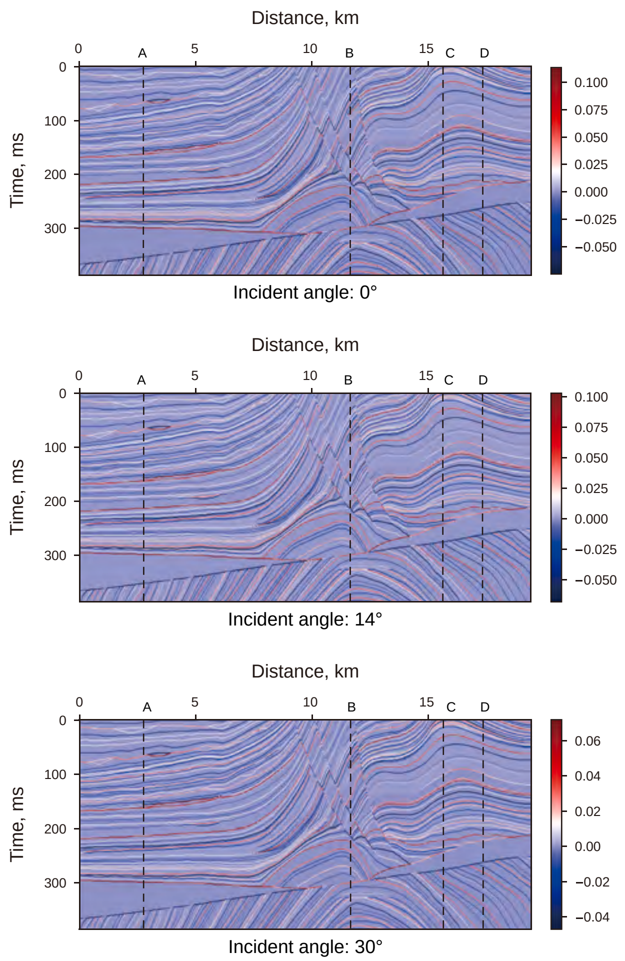

Fig. 6. True reflectivity models at incident angles of 0°, 14°, and 30°. Black dashed lines denote well locations.

network. Well-log data are used to construct training datasets based on the Zoeppritz equation for broadening the frequency bandwidth of pre-stack seismic data and preserving AVO relationships during enhancing resolution. Additionally, the convolution model is incorporated into the training stage for enhancing the generalizability by using unlabeled seismic data. By integrating these multi-source data and physical models under a semi-supervised learning framework, the proposed method is capable of enhancing the resolution of pre-stack seismic data and preserving AVO relationships through alleviating the wavelet tuning effect. In addition, the proposed method is both effective and

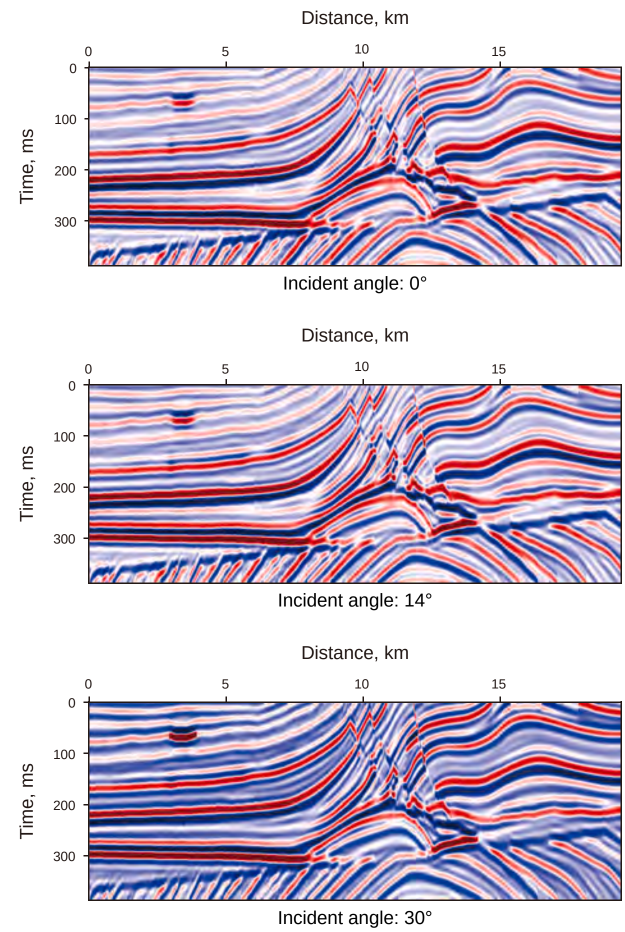

Fig. 8. Synthetic seismic data with frequency band of 0–10–40–60 Hz.

straightforward to implement, as demonstrated by experiments on both synthetic data and three-dimensional field data.

2. Methods

2.1. The AVO-preserved pre-stack seismic data resolution enhancement method

To facilitate a clearer understanding of the specific problem that our proposed method is designed to address, a brief overview of the wavelet tuning effect is first presented. The wavelet tuning effect refers to the phenomenon where, when seismic waves encounter very thin layers, the reflected waves generated from the

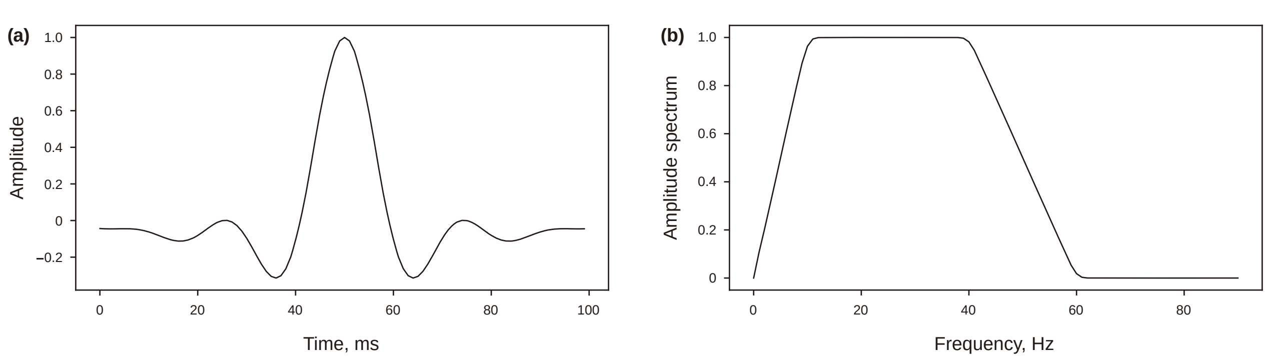

Fig. 7. **(a)** The wavelet with frequency band of 0–10–40–60 Hz and **(b)** its frequency spectrum.

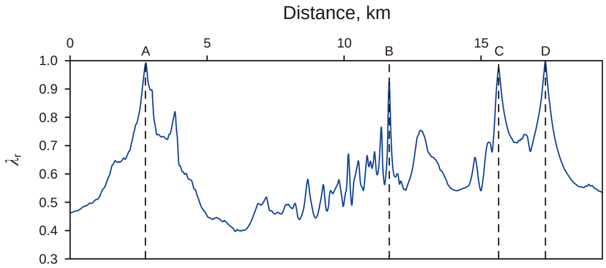

Fig. 9. The distribution of weight coefficients λ_r.

Table 1
RMSE and PCC between the results processed by proposed method and the true high-resolution data, and training time of proposed method, for inputting 1, 3, 5, and 7 AVA gathers.

	1 trace	3 traces	5 traces	7 traces
RMSE	0.0186	0.0184	0.0180	0.0178
PCC	0.9118	0.9133	0.9182	0.9185
Training time	42 s	52 s	61 s	72 s

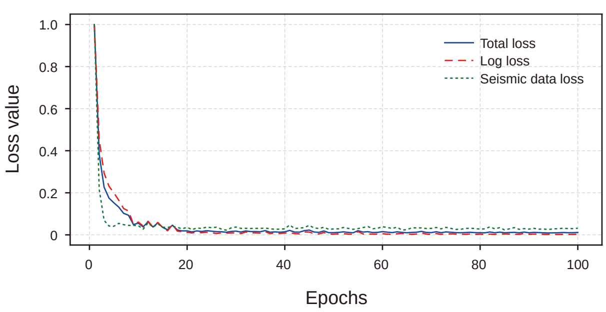

Fig. 10. Loss function convergence curves of the proposed method.

Table 2
Computational efficiency of different methods when processing synthetic data.

	Deconvolution method	Pure data-driven method	Proposed method	U-net based method
Training time	27 s	10 s	61 s	4 h
Inference time	-	0.8 s	0.8 s	8s

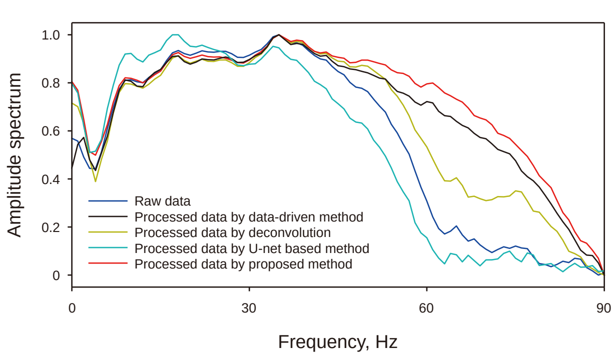

Fig. 11. Comparisons of frequency spectra of raw seismic data and processed seismic data.

Table 3
The ratio of the amplitude spectra after normalization between the processed data and the original synthetic data.

	Deconvolution method	Pure data-driven method	Proposed method	U-net based method
0–10 Hz	0.95	0.98	1.15	1.20
10–40 Hz	0.95	0.99	0.99	1.01
40–90 Hz	1.26	1.67	1.84	0.70

top and bottom interfaces of the thin layer interfere with each other. This interference leads to changes in the amplitude, frequency, and waveform of the reflected wave on seismic records. This phenomenon is related to the thickness of the subsurface layer, as well as the wavelet's shape and bandwidth. For a clearer illustration, a synthetic data experiment is designed. Fig. 1 shows an elastic model comprising three adjacent thin low-velocity layers and one thick high-velocity layer. And Fig. 2 shows the simulated amplitude variation with angle (AVA) gathers using different wavelets with frequency bandwidths of 3–30 Hz and 3–80 Hz based on the Zoeppritz equation (Zoeppritz, 1919). For the thick high-velocity layer, 3–80 Hz AVA gathers exhibit a more accurate and clearer boundary, compared to 3–30 Hz AVA gathers. For thin low-velocity layers, due to tuning effects, the simulated AVA data using a wavelet with bandwidth of 3–30 Hz cannot resolve the top and bottom boundaries of the first two thin layers, exhibiting Class IV AVO characteristics in the AVA gathers. However, when the wavelet frequency is enhanced, the simulated AVA data using a wavelet with bandwidth of 3–80 Hz clearly delineated the top and bottom boundaries of these two thin layers, exhibiting Class I AVO characteristics as shown in Fig. 2(c) and (d). Therefore, preserving true AVO relationships during pre-stack seismic data resolution enhancement is a crucial task, as it aids in clearer and more accurate identification of subsurface thin layers.

For mitigating the wavelet tuning effect and preserve true AVO relationships during resolution enhancement, the AVO-preserved pre-stack seismic data resolution enhancement method is proposed under a semi-supervised learning framework. In the proposed method, the neural network is designed to build the mapping relationship between pre-stack AVA gathers and subsurface reflection coefficients, which can be expressed as:

$$\mathbf{R}_{\text{angle}} = G\left(\mathbf{d}_{\text{angle}}\right), \tag{1}$$

where G represents the neural network, $\mathbf{d}_{\text{angle}}$ represents the pre-stack AVA gathers, $\mathbf{R}_{\text{angle}}$ represents the corresponding reflection coefficients.

To avoid reliance on large labelled datasets for neural network training while preserving AVO relationships during resolution enhancement, we design our method under a semi-supervised learning framework, incorporating both the convolution model and the Zoeppritz equation into the training process. A semi-supervised learning framework comprises two parts: one supervised learning part and one self-supervised learning part. The supervised learning part is based on the labelled dataset built by well-log data, corresponding AVA gathers, and the Zoeppritz equation. The loss function of the supervised learning part can be expressed as

$$\text{loss}_{\text{r}} = \left\| Z\left(\mathbf{m}_{\log}\right) - G\left(\mathbf{d}_{\text{angle}}\right) \right\|, \tag{2}$$

where Z donotes the Zoeppritz equation and $\mathbf{m}_{\log}$ represents the elastic parameters derived from the well-log data. Well-log data derived from the directly measurement of subsurface model are typically the highest resolution data available to us. The

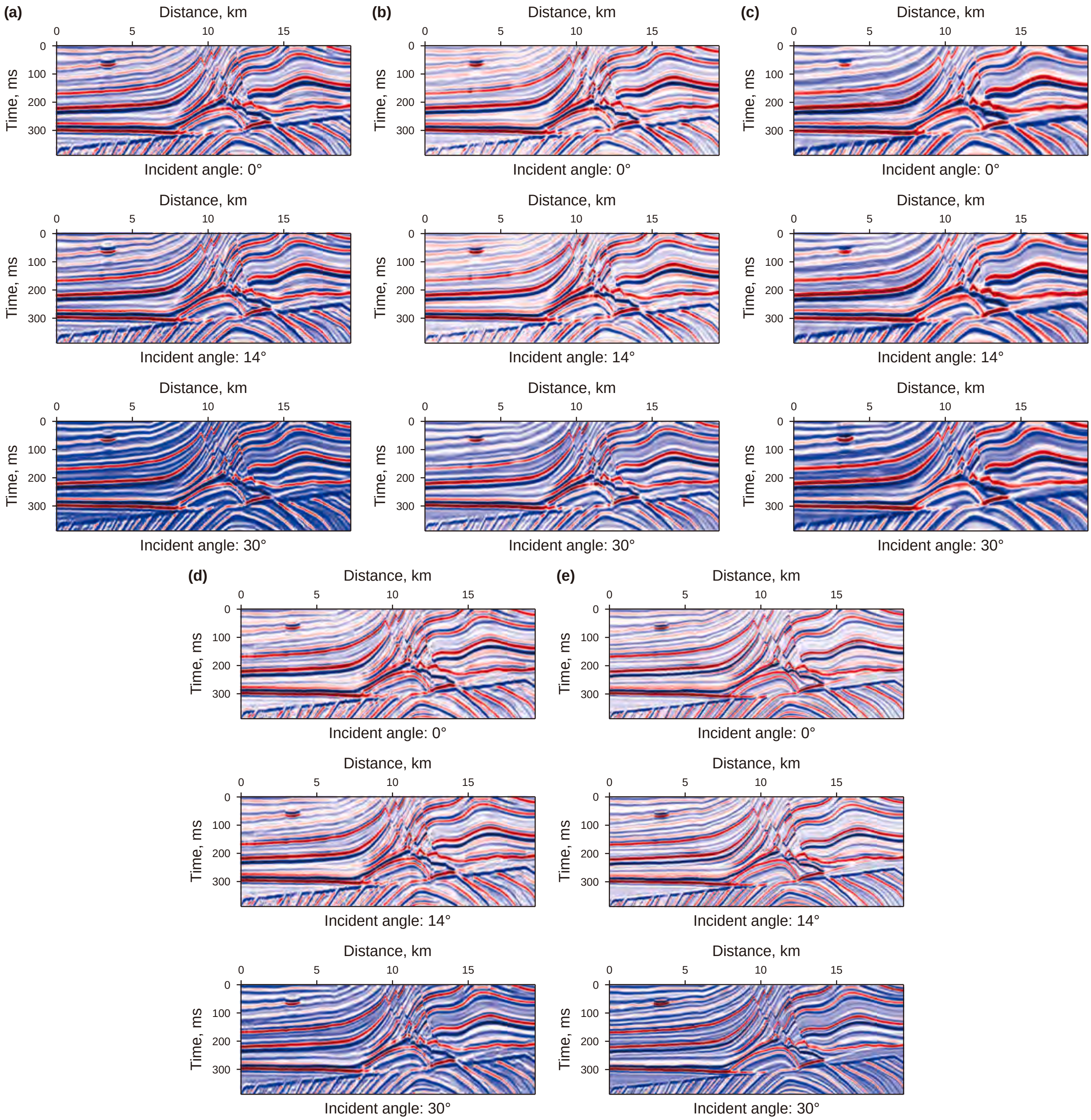

Fig. 12. Resolution-enhanced seismic data of 0°, 14° and 30° incident angle obtained by **(a)** deconvolution, **(b)** pure data-driven method, **(c)** the U-net based method, **(d)** the proposed method, and **(e)** the true 0–3–60–90 Hz seismic data of 0°, 14° and 30° incident angle.

supervised learning part is designed to equip the neural network with the capability to suppress wavelet tuning effect in pre-stack seismic data using well-log data. This ensures the fidelity of AVO relationships during the resolution enhancement.

For supervised learning part, labelled datasets are derived from well-log data. However, well-log data are often quite sparse in the field exploration. Consequently, in this scenario, supervised learning-trained neural networks tend to have poor generalization. To enhance its generalizability, in the proposed method, the neural network is also trained using self-supervised learning diagram simultaneously, leveraging massive unlabeled AVA gathers to update parameters of the neural network. For this self-supervised learning part, the convolution model is integrated into the neural network training process. The wavelet employed within the convolution model is derived directly from the seismic data. It is imperative that the wavelet's frequency bandwidth closely matches that of the seismic data, thereby ensuring that information within the original data bandwidth is not lost during resolution enhancement. The loss function of the self-supervised learning part can be expressed as

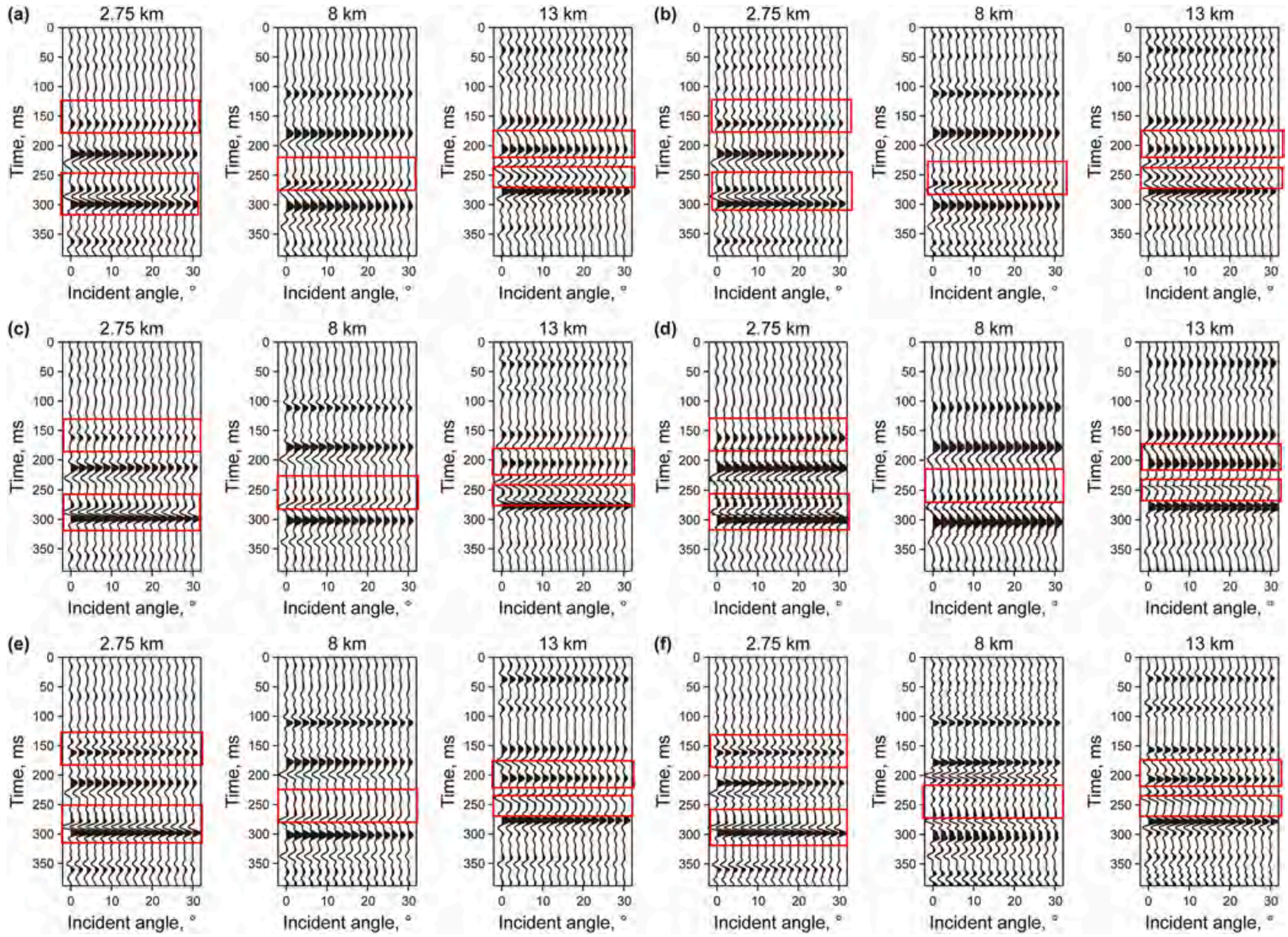

Fig. 13. Comparisons of AVA gathers located at 2.75 km (the well A location), 8 km and 13 km. **(a)** The original AVA gathers with frequency band of 0–10–40–60 Hz; **(b)** the AVA gathers processed by deconvolution; **(c)** the AVA gathers processed by pure data-driven method; **(d)** the AVA gathers processed by the U-net based method; **(e)** the AVA gathers processed by the proposed method; **(f)** the true high-resolution AVA gathers with frequency band of 0–3–60–90 Hz.

$$\mathrm{loss_d} = \left\| \mathrm{Conv}\left(G\left(\mathbf{d}_{\mathrm{angle}}\right), \mathbf{w}\right) - \mathbf{d}_{\mathrm{angle}} \right\|, \tag{3}$$

where Conv denotes the convolution model and $\mathbf{w}$ denotes the wavelet. Due to the automatic differentiation mechanism of neural networks, the self-supervised learning part effectively is equal to the deconvolution on the seismic data by optimizing parameters of the neural network. Through weighting $\mathrm{loss_d}$ and $\mathrm{loss_r}$, the total loss $\mathrm{loss_t}$ is obtained, which can be expressed as:

$$\mathrm{loss_t} = \lambda_{\mathrm{r}}\mathrm{loss}_{\mathrm{r}} + \lambda_{\mathrm{d}}\mathrm{loss}_{\mathrm{d}}, \tag{4}$$

λ_{r} and λ_{d} are weight coefficients for the well-log data loss and seismic data loss respectively, with the constraint that $\lambda_{\mathrm{r}} + \lambda_{\mathrm{d}} = 1$. λ_{r} and λ_{d} influence the accuracy of the inversion results. To better leverage the well-log data for constraining the inversion, we employ the weighting method proposed by Wu et al. (2024) that combines the correlation of seismic data with the distance between different traces. We make some modifications to the method proposed by Wu et al. (2024), specifically by using the grey correlation analysis, rather than the Pearson correlation coefficient, to measure the degree of similarity between data, as it does not rely on strict assumptions on data distribution (Deng, 1982; Kuo et al., 2008), making it more suitable for seismic data. The calculation formula of grey relational analysis is as follows:

$$\mathrm{GC}\left(\mathbf{d}_{uj}^{k}, \mathbf{d}_{lj}^{m}\right) = \sum_{j=0}^{\mathrm{NT}} \frac{\min\limits_{k}\min\limits_{j}\left|\mathbf{d}_{uj}^{k} - \mathbf{d}_{lj}^{m}\right| + \rho\max\limits_{j}\max\limits_{k}\left|\mathbf{d}_{uj}^{k} - \mathbf{d}_{lj}^{m}\right|}{\left|\mathbf{d}_{uj}^{k} - \mathbf{d}_{lj}^{m}\right| + \rho\max\limits_{j}\max\limits_{k}\left|\mathbf{d}_{uj}^{k} - \mathbf{d}_{lj}^{m}\right|}, \tag{5}$$

where $\mathrm{GC}\left(\mathbf{d}_{uj}^{k}, \mathbf{d}_{lj}^{m}\right)$ is the correlation value of grey relational analysis between k-th seismic trace and the m-th seismic trace. $\mathbf{d}_{uj}^{k}$ represents the amplitude value of the j-th time sample on the k-th unlabeled seismic trace and $\mathbf{d}_{lj}^{m}$ represents the amplitude value of the j-th time sample on the m-th labelled seismic trace. ρ is an adjustable coefficient used to modulate the magnitude of the difference in the output results, assigned a value of 0.5 usually.

$$\mu_j = \max_{i}\mathrm{GC}\left(\mathbf{d}_{uj}^{k}, \mathbf{d}_{lj}^{m}\right) * \frac{1}{D_i^j}, \tag{6}$$

where D_i^j denotes the distance between the k-th unlabeled seismic trace and the m-th labelled seismic trace. Finally, we obtain the weight of well-log data loss λ_{r} by normalizing μ_j. We use maximum-minimum normalization:

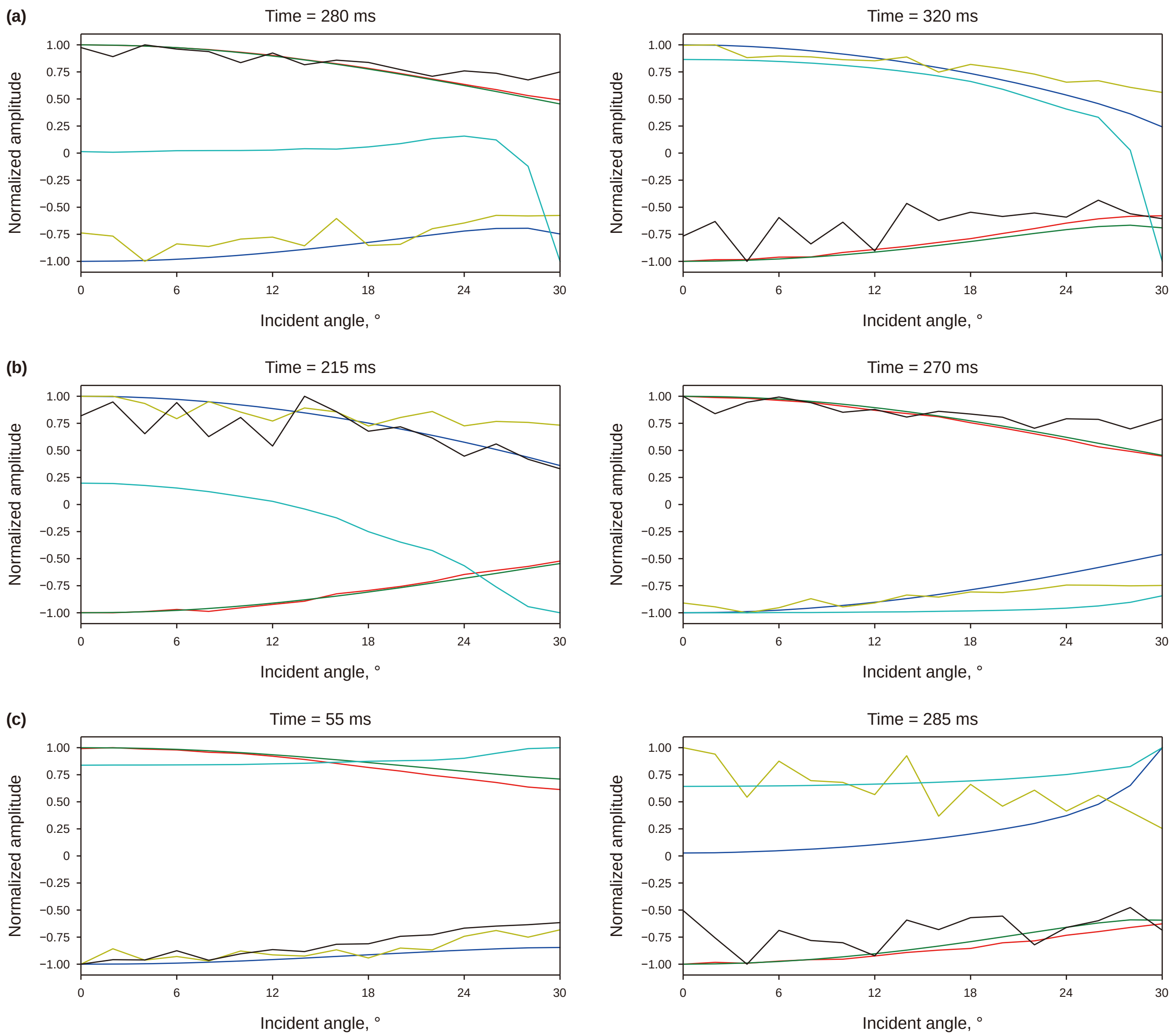

Fig. 14. AVO relationships of pre-stack seismic data located at **(a)** 2.75 km (the well A location), **(b)** 8 km and **(c)** 13 km. Blue lines denote raw 0–10–40–60 Hz seismic data; green lines denote true 0–3–60–90 Hz seismic data calculated based on the true model; yellow lines denote processed seismic data by deconvolution; black lines denote processed seismic data by pure data-driven method; cyan lines denote processed seismic data by U-net based method; red lines denote processed seismic data by the proposed method.

$$\lambda_r = \frac{\mu_j - \mu_{j\mathrm{min}}}{\mu_{j\mathrm{max}} - \mu_{j\mathrm{min}}}, \tag{7}$$

And then the weight of seismic data loss can be calculated by $\lambda_\mathrm{d} = 1 - \lambda_\mathrm{r}$.

Within this semi-supervised learning framework, the neural network is simultaneously trained under the constraints of well-log data, massive AVA gather data, the Zoeppritz equation, and the convolution model. This integration of multi-source data and physical models enables the network, once trained, to enhance the resolution of pre-stack seismic data and preserve AVO relationships. Subsequently, inputting AVA gathers into the trained neural network directly produces the resolution-enhanced AVA gathers.

The flowchart of our method is illustrated in Fig. 3. The solid line represents the forward propagation of the neural network, while the dotted line represents the backward propagation. First, the real reflection coefficients at different incident angles $\mathbf{r}_\mathrm{l}$ are derived from the well-log data according to the Zoeppritz equation, and the corresponding seismic data $\mathbf{d}_\mathrm{l}$ at the well location are used to build the labelled dataset, and the seismic data $\mathbf{d}_\mathrm{u}$ at the non-well location serve as unlabeled data. When the neural network starts training, labelled seismic data $\mathbf{d}_\mathrm{l}$ are input into the neural network to obtain the reflection coefficient $\dot{\mathbf{r}}_\mathrm{l}$ output by the network. Based on the labelled reflection coefficient $\mathbf{r}_\mathrm{l}$ at the well location, the loss of the well-log data loss_r at the well location is calculated; the unlabeled seismic data $\mathbf{d}_\mathrm{u}$ is input into the neural network, and the network outputs reflection coefficients model $\dot{\mathbf{r}}_\mathrm{u}$. The seismic wavelet and convolution model are incorporated as a physical model constraint of the neural network, enabling the simulated seismic data $\dot{\mathbf{d}}_\mathrm{u}$ from $\dot{\mathbf{r}}_\mathrm{u}$ and unlabeled seismic data $\mathbf{d}_\mathrm{u}$ can construct the seismic data loss (loss_d) to train the network. The total loss (loss_t) is obtained by weighting loss_d and loss_r. During the training stage, the parameters of the neural network are updated by optimizing the loss_t. Once the training stage finished, all AVA gathers are input into the neural network to get the high-resolution AVA gathers.

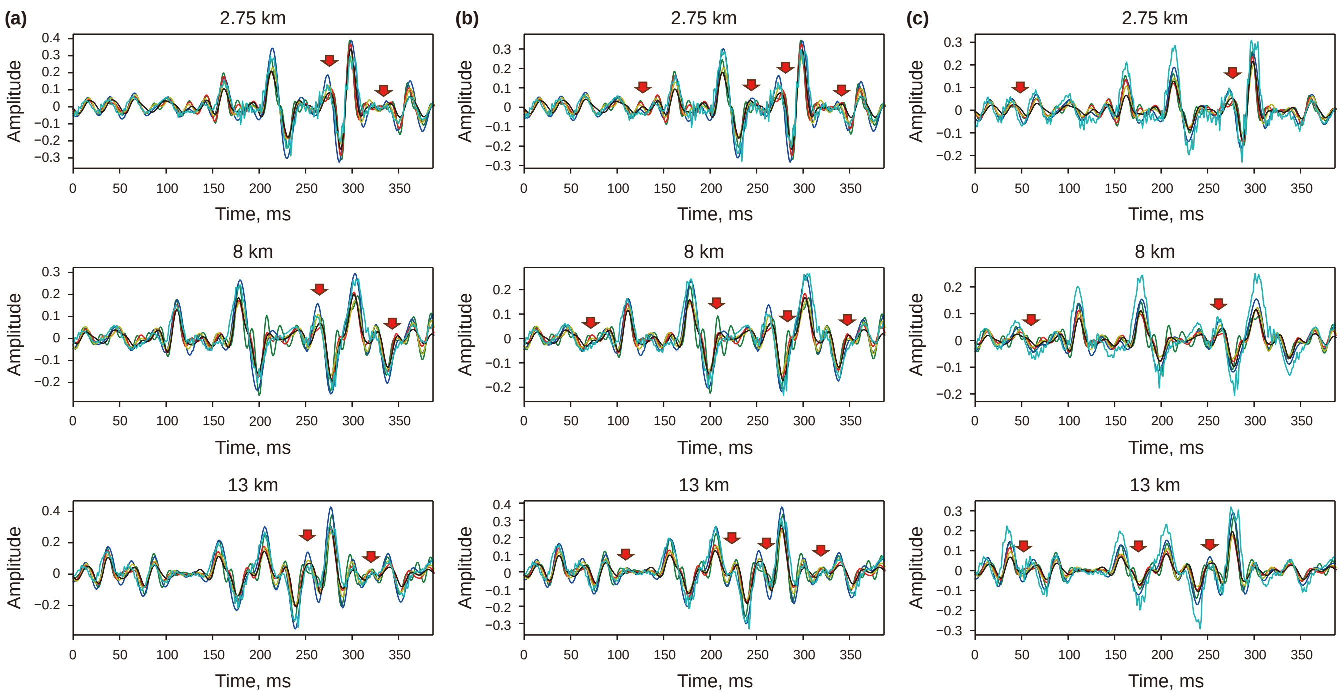

Fig. 15. Comparisons of the single trace data with incident angles of 0°, 14° and 30° located at 2.75 km (the well A location),8 km and 13 km. **(a)** Comparisons of seismic data with 0° incident angle; **(b)** comparisons of seismic data with 14° incident angle; **(c)** comparisons of seismic data with 30° incident angle. Blue lines denote raw 0–10–40–60 Hz seismic data; green lines denote true 0–3–60–90 Hz seismic data; yellow lines denote processed seismic data by deconvolution; black lines denote processed seismic data by pure data-driven method; cyan lines denote processed seismic data by U-net based method; red lines denote processed seismic data by the proposed method.

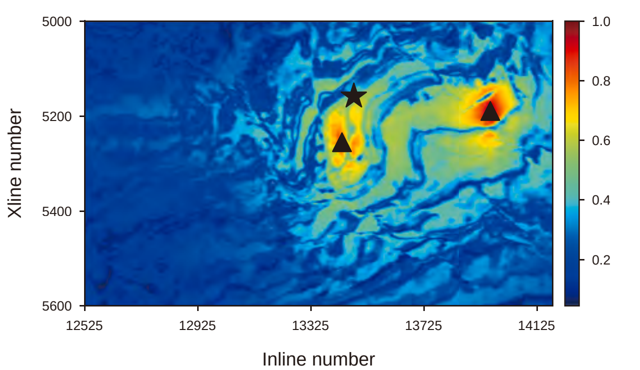

Fig. 16. The distribution of weight coefficients λ_r. Black triangles represent locations of training wells and the pentagram represents the location of the blind well.

2.2. The structure of the neural network

In the proposed method, neural networks are used to integrate pre-stack seismic data and well-log data by establishing a mapping between AVA seismic data and reflection coefficients via incident angles. AVA seismic data are time-sequence data and reveal spatial features of the subsurface model. To extract these features from the AVA seismic data, we design a neural network architecture (Fig. 4) that utilizes recurrent neural networks with 16 hidden sizes and 5 layers for sequence feature extraction, the channel attention and convolution neural networks with 5 × 5 kernel for spatial feature extraction. Sequence features extracted by the RNN and spatial features extracted by the CNN are concatenated along the channel dimension. Subsequently, channel attention is applied to these combined features, weighting them along the channel dimension to enhance the importance of key

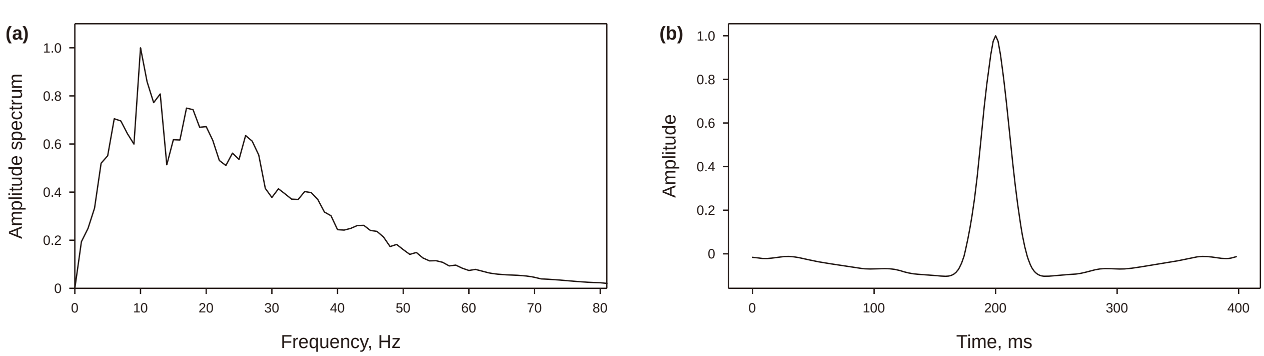

Fig. 17. **(a)** The frequency spectra of the raw pre-stack seismic data and **(b)** the wavelet derived from (a) by inverse Fourier transform.

Table 4
Computational efficiency of different methods when processing synthetic data.

	Deconvolution method	Pure data-driven method	Proposed method	U-net based method
Training time	5 h	31 s	11 h	4 h
Inference time	-	540 s	540 s	1 h

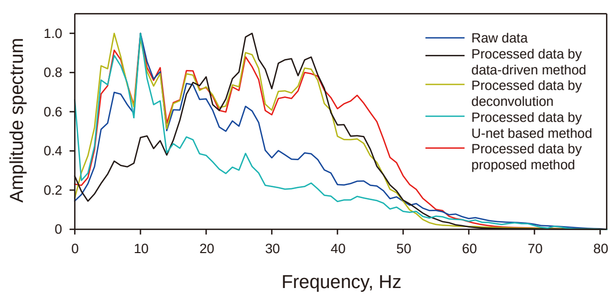

Fig. 18. Frequency spectra of raw seismic data and processed seismic data.

Table 5
The ratio of the amplitude spectra after normalization between the processed data and the original field data.

	Deconvolution method	Pure data-driven method	Proposed method	U-net based method
0–10 Hz	1.43	0.48	1.29	1.43
10–30 Hz	1.16	1.03	1.15	0.67
30–60 Hz	1.93	2.16	2.49	0.59

features. After this channel attention, the data passes through two convolution neural networks with 3 × 3 kernel and a deconvolution neural network with 5 × 5 kernel to extraction features further, and then a fully connected layer is used to ultimately obtain reflection coefficients that vary with the incident angle.

3. Synthetic data examples

To verify the effectiveness of the proposed method, we tested it on the Marmousi2 model, as shown in Fig. 5. This model comprises of a total of 1943 traces, with 387 sampling points, a 10 m spacing between each trace, and 1 ms sampling interval. Reflectivity models via angles are derived based on the Zoeppritz equation, which is shown in Fig. 6. A broadband wavelet with a frequency band of 0–10–40–60 Hz, which is shown in Fig. 7, is used to generate the AVA gather data based on the convolution model. The synthetic pre-stack seismic data are shown in Fig. 8. We selected four traces as pseudo-logs for data resolution enhancement, located at 2.75, 11.65, 15.64, and 17.35 km, as indicated by black dashed lines in Figs. 5 and 6. To apply our proposed joint data- and model-driven resolution enhancement method, we need to calculate the λ_r in our proposed method, which is shown in Fig. 9 and set a reasonable target of resolution enhancement. Based on the analysis of the frequency band of the synthetic AVA gather data, we set the resolution enhancement target to 0–3–60–90 Hz. To maintain horizontal consistency of the processed data, multiple consecutive AVA gathers are fed into the neural network. Table 1 presents the root mean square error (RMSE) and Pearson correlation coefficient (PCC) between the results processed by our method and the true high-resolution data for input AVA gathers of 1, 3, 5, and 7. Considering that increasing the number of input gathers leads to higher computational costs, we chose to use five consecutive trace gathers to balance performance and efficiency.

To demonstrate the effectiveness of our method, we enhance the resolution of these synthetic pre-stack seismic data using our method, the deconvolution method, pure data-driven method and U-net based resolution enhancement method (Li et al., 2022). The purely data-driven method is essentially our proposed method with the physical model removed. And the U-Net-based resolution enhancement method employs the weights provided by Li et al. (2022) in their publication. All experiments are performed using an Intel(R) Xeon(R) Gold 6130 CPU clocked at 2.10 GHz and an NVIDIA Tesla V100 GPU equipped with 32 GB of VRAM. For both our proposed method and the data-driven approach, training is performed with a batch size of 128 using the Adam optimizer, and a learning rate of 0.03 with 1e−4 decay. An early stopping strategy is employed to prevent overfitting, terminating training if the total loss function shows no decrease for 10 consecutive epochs.

Fig. 10 displays loss function convergence curves of the proposed method, demonstrating a stable decrease in the total loss function, as well as in the individual loss components for the well logs and seismic data. Furthermore, it also reveals that our method effectively balances the seismic data and well-log losses, leading to the stable and concurrent decrease of both components. Moreover, this observation underscores the robustness of our proposed semi-supervised learning method, as it achieves stable loss function convergence without necessitating overly intricate hyper-parameter tuning. Table 2 summarizes the computational time required for various processing methods. Although our method is comparatively more time-consuming for training, it offers superior inference efficiency when contrasted with single-angle processing techniques, such as the U-net based method.

Fig. 11 shows frequency spectra of the raw data and processed data by different methods. Processed by our method, the frequency band of the data is broadened to 0–3–60–90 Hz, as shown in Fig. 11, while the processed data by other methods exhibit a narrower frequency band and lower energy in high frequencies. The spectra are divided into three frequency bands based on the original data's frequency range: 0–10 Hz, 10–40 Hz (the dominant frequency band of the original data), and 40–90 Hz. After normalizing the amplitude spectral energy, the ratio of the amplitude spectral energy of the resolution-enhanced data to that of the original data is calculated, with the results presented in Table 3. Our proposed method, when compared to the original data, demonstrates an enhancement in both low, and high-frequency energy while preserving the energy within the dominant frequency band of original data. Notably, in the high-frequency band, our method achieves a 1.8-fold increase in amplitude spectral energy, which is the highest improvement compared to other methods. Fig. 12 shows the processed seismic data and the high-resolution seismic data calculated based on the true elastic model (with a frequency band of 0–3–60–90 Hz) at incident angles of 0°, 14°, and 30°. Compared to the raw seismic data and processed data by other methods, processed data by our method exhibit higher resolution.

Additionally, as shown in Fig. 13, comparisons of AVA gathers located at 2.75 km (the well A location), 8 km, and 13 km demonstrate that, regardless of the proximity to the well location, our method can effectively enhance the resolution of pre-stack data and maintain AVO relationships of pre-stack seismic data, especially in the regions highlighted by the red boxes. Fig. 14 presents AVO relationships in pre-stack seismic data located at 2.75 km (the well A location), 8 km, and 13 km. Although all resolution enhancement methods are able to enhance the resolution of pre-stack data. However, with the exception of the purely data-driven approach and our proposed method, other resolution

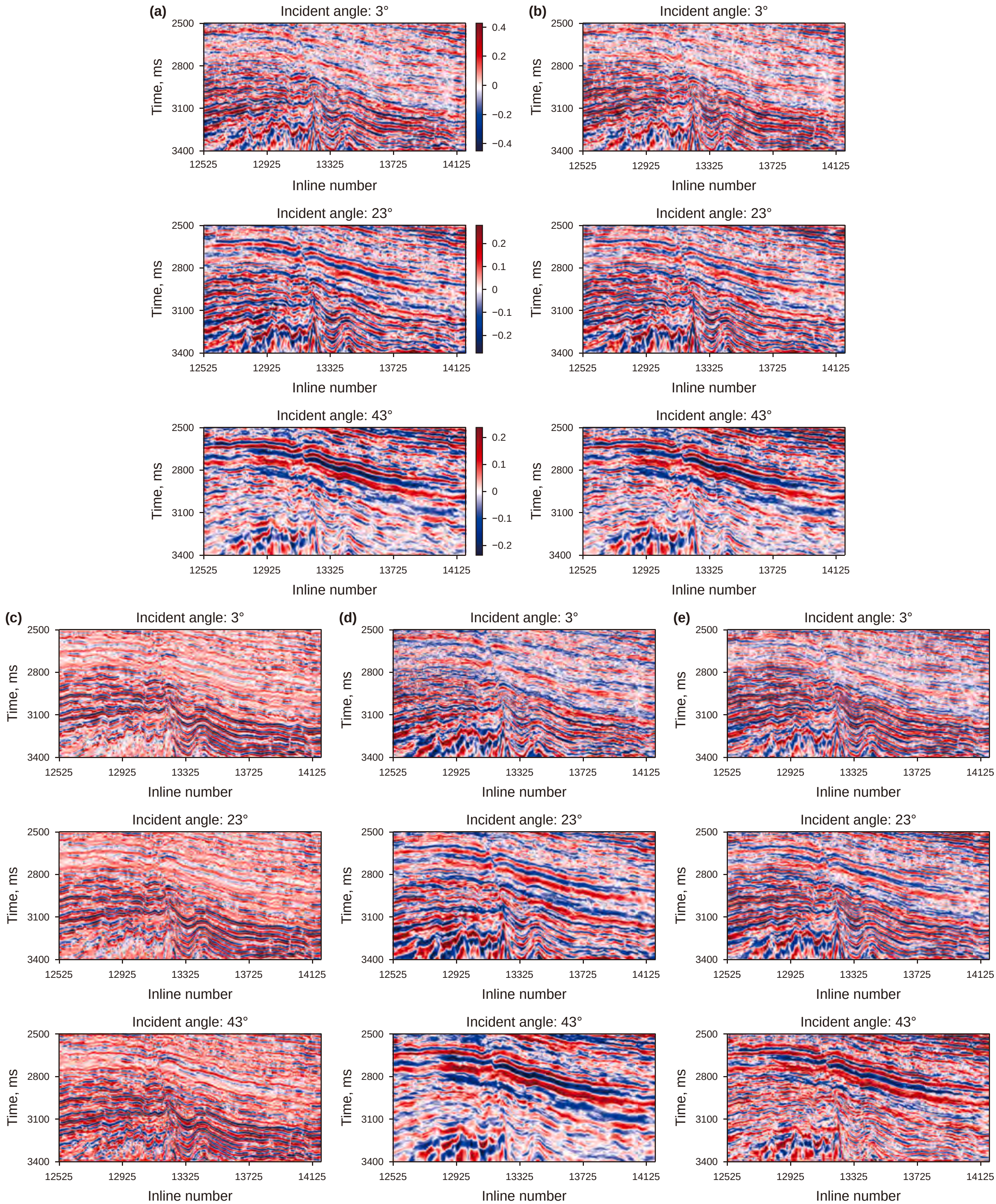

Fig. 19. Comparisons of the pre-stack seismic data of Xline 5255 with incident angles of 3°, 23° and 43°. **(a)** Raw pre-stack seismic data; **(b)** the pre-stack seismic data processed by deconvolution; **(c)** the pre-stack seismic data processed by pure data-driven method; **(d)** the pre-stack seismic data processed by U-net based method; **(e)** the pre-stack seismic data processed by the proposed method.

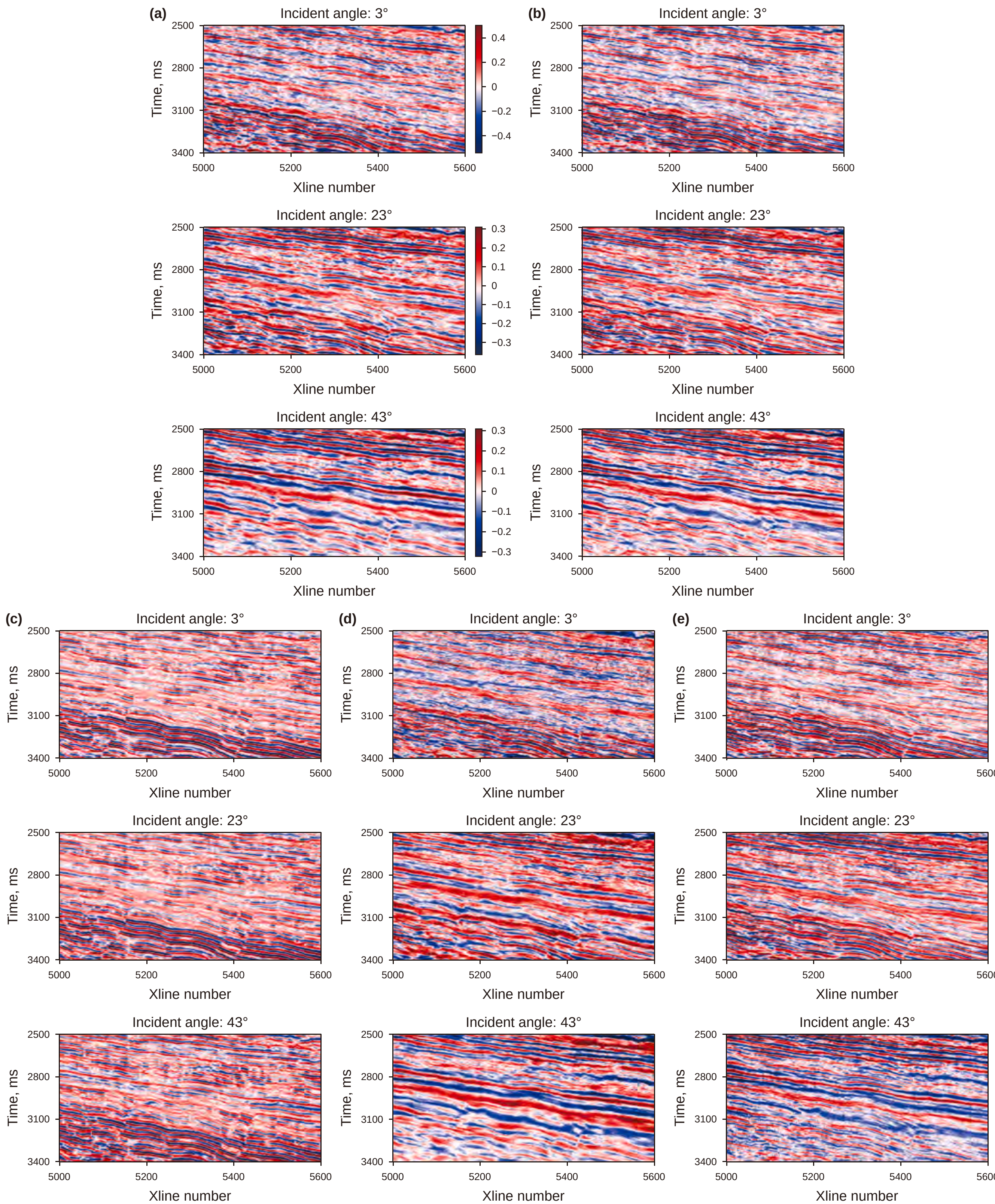

Fig. 20. Comparisons of the pre-stack seismic data of Inline 13,960 with incident angles of 3°, 23° and 43°. (**a**) Raw pre-stack seismic data; (**b**) the pre-stack seismic data processed by deconvolution; (**c**) the pre-stack seismic data processed by pure data-driven method; (**d**) the pre-stack seismic data processed by U-net based method; (**e**) the pre-stack seismic data processed by the proposed method.

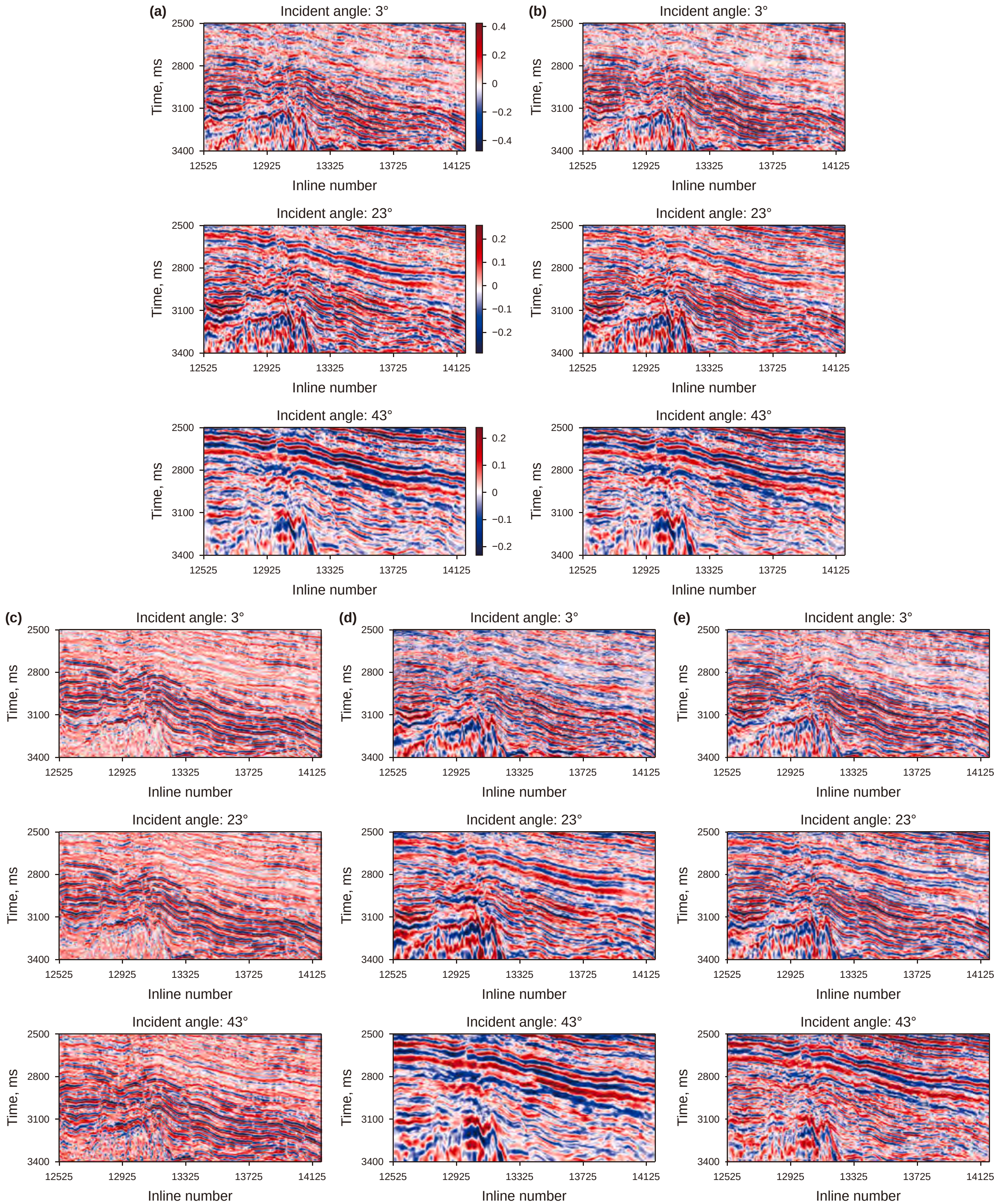

Fig. 21. Comparisons of the pre-stack seismic data of Xline 5158 with incident angles of 3°, 23° and 43°. **(a)** Raw pre-stack seismic data; **(b)** the pre-stack seismic data processed by deconvolution; **(c)** the pre-stack seismic data processed by pure data-driven method; **(d)** the pre-stack seismic data processed by U-net based method; **(e)** the pre-stack seismic data processed by the proposed method.

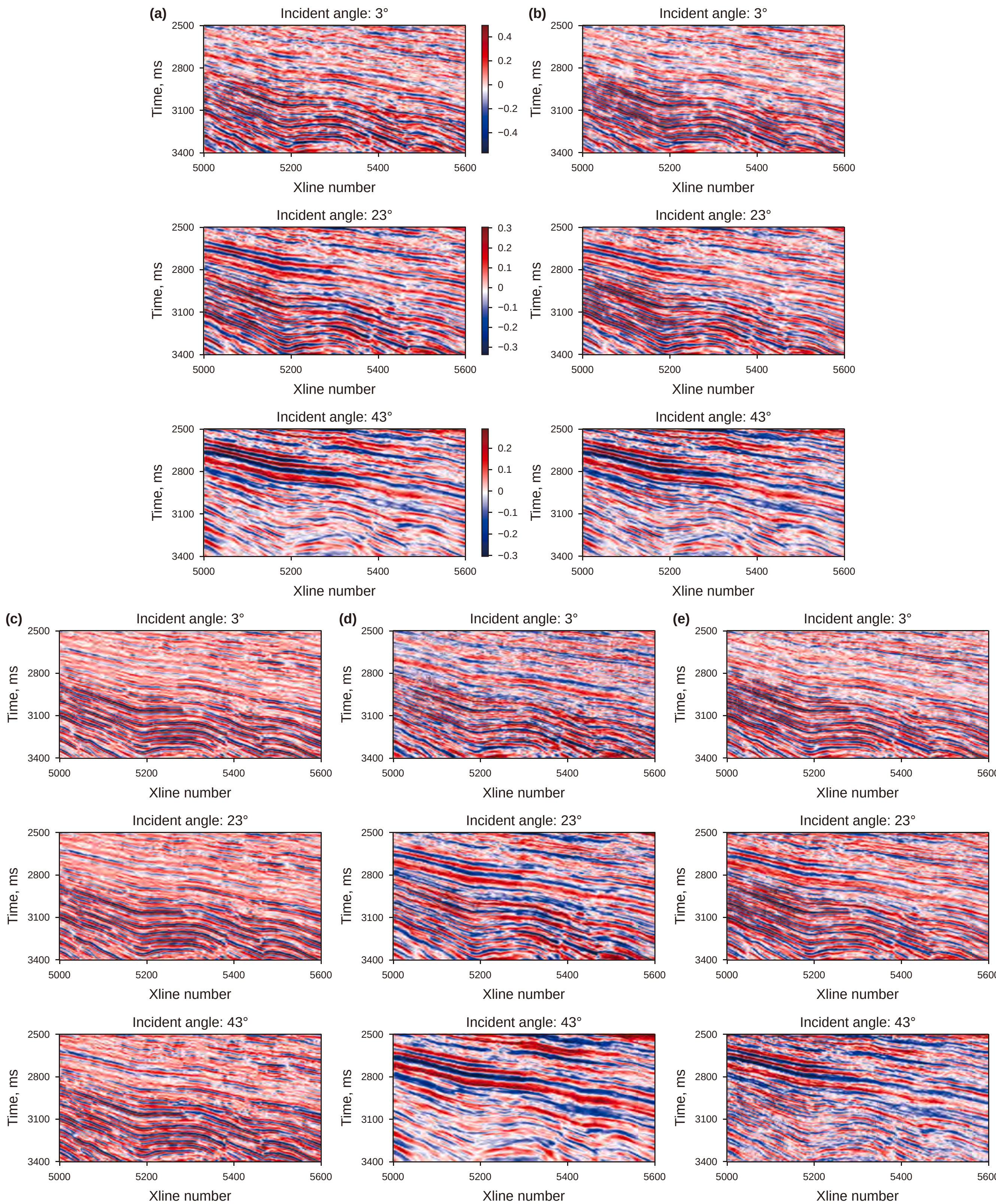

Fig. 22. Comparisons of the pre-stack seismic data of Inline 13,477 with incident angles of 3°, 23° and 43°. (**a**) Raw pre-stack seismic data; (**b**) the pre-stack seismic data processed by deconvolution; (**c**) the pre-stack seismic data processed by pure data-driven method; (**d**) the pre-stack seismic data processed by U-net based method; (**e**) the pre-stack seismic data processed by the proposed method.

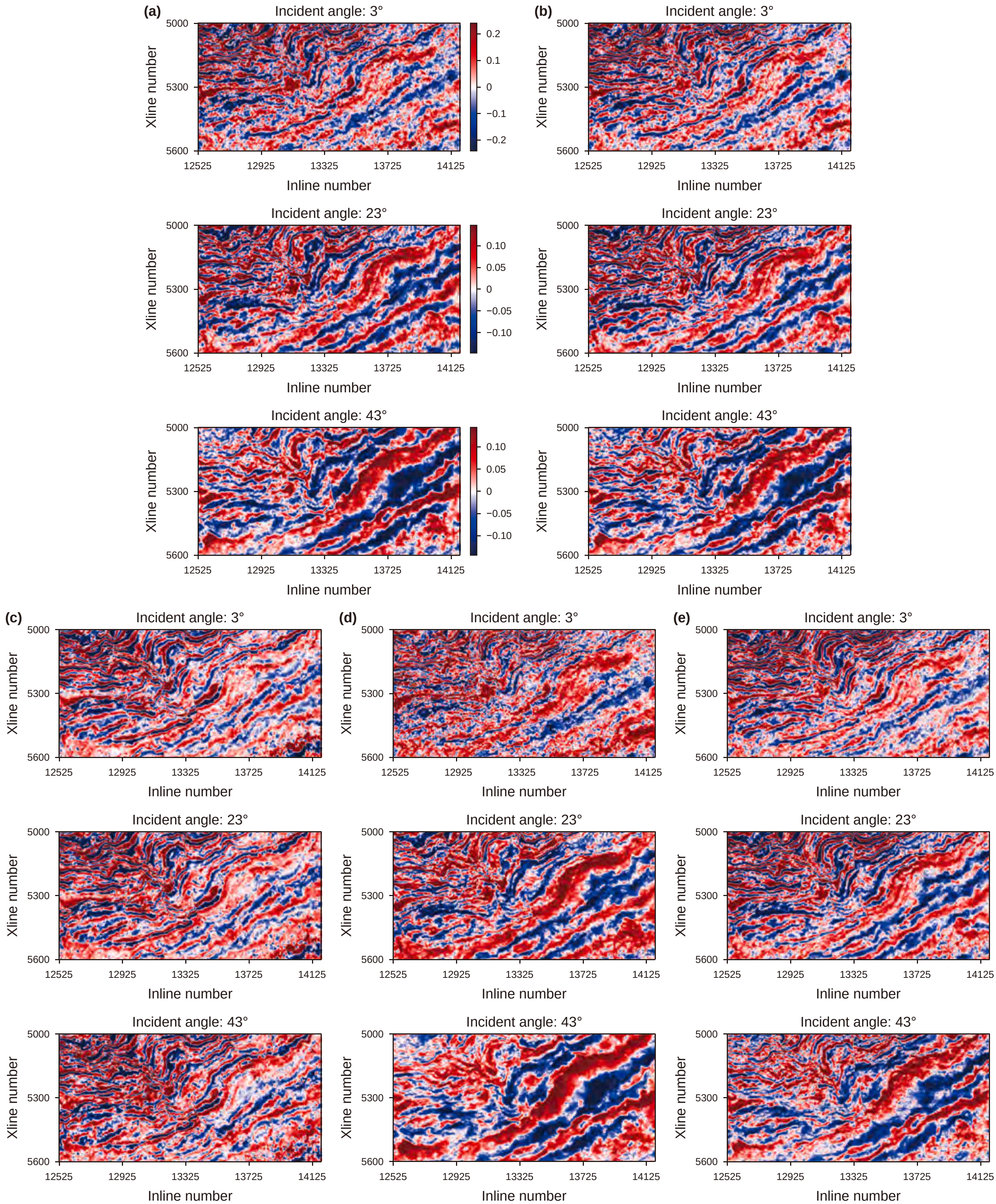

Fig. 23. Time slices (time = 2900 ms) of pre-stack seismic data at incident angles of 3°, 23° and 43°. **(a)** Raw pre-stack seismic data; **(b)** the pre-stack seismic data processed by deconvolution; **(c)** the pre-stack seismic data processed by pure data-driven method; **(d)** the pre-stack seismic data processed by U-net based method; **(e)** the pre-stack seismic data processed by the proposed method.

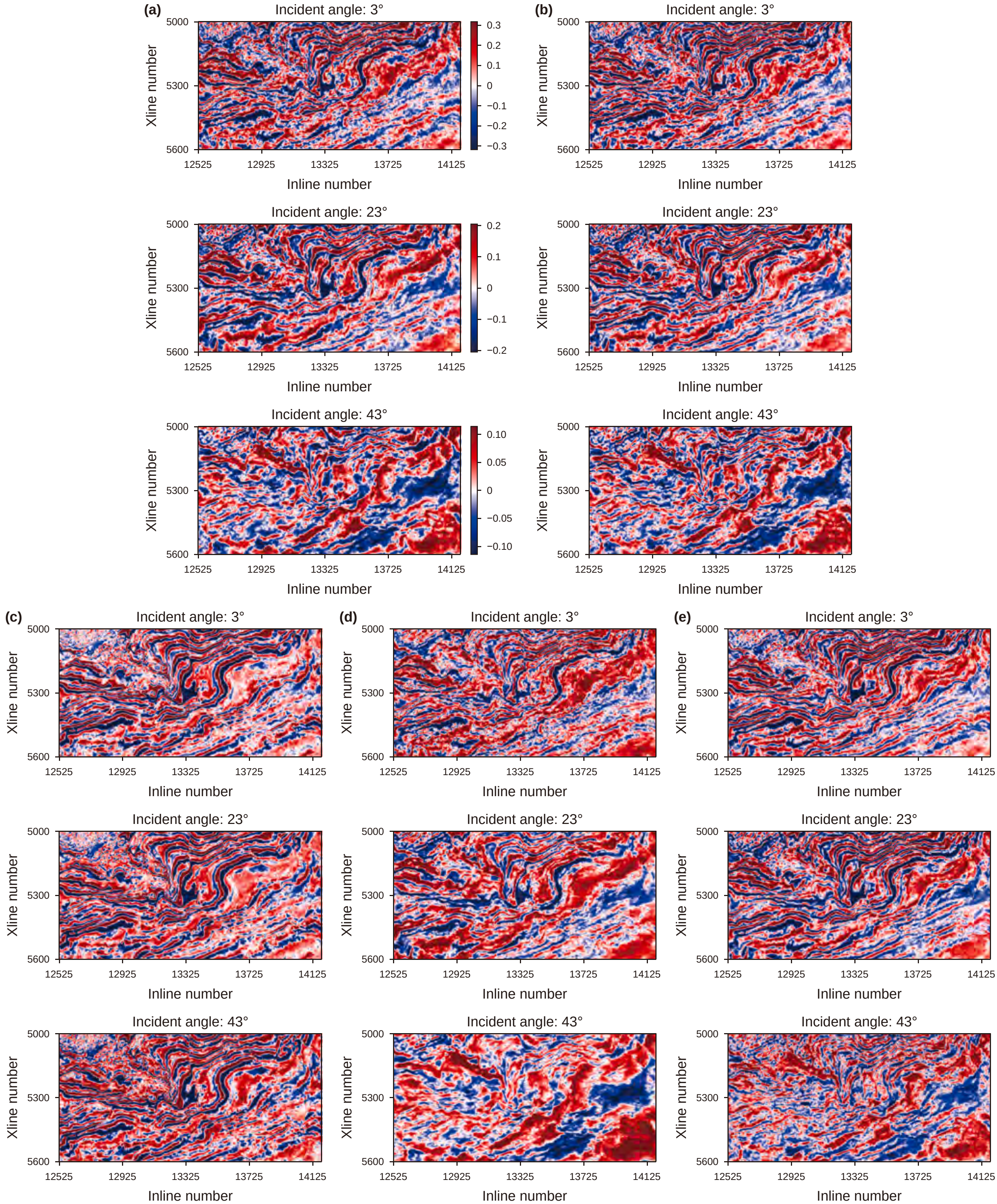

Fig. 24. Time slices (time = 3100 ms) of pre-stack seismic data at incident angles of 3°, 23° and 43°. **(a)** Raw pre-stack seismic data; **(b)** the pre-stack seismic data processed by deconvolution; **(c)** the pre-stack seismic data processed by pure data-driven method; **(d)** the pre-stack seismic data processed by U-net based method; **(e)** the pre-stack seismic data processed by the proposed method.

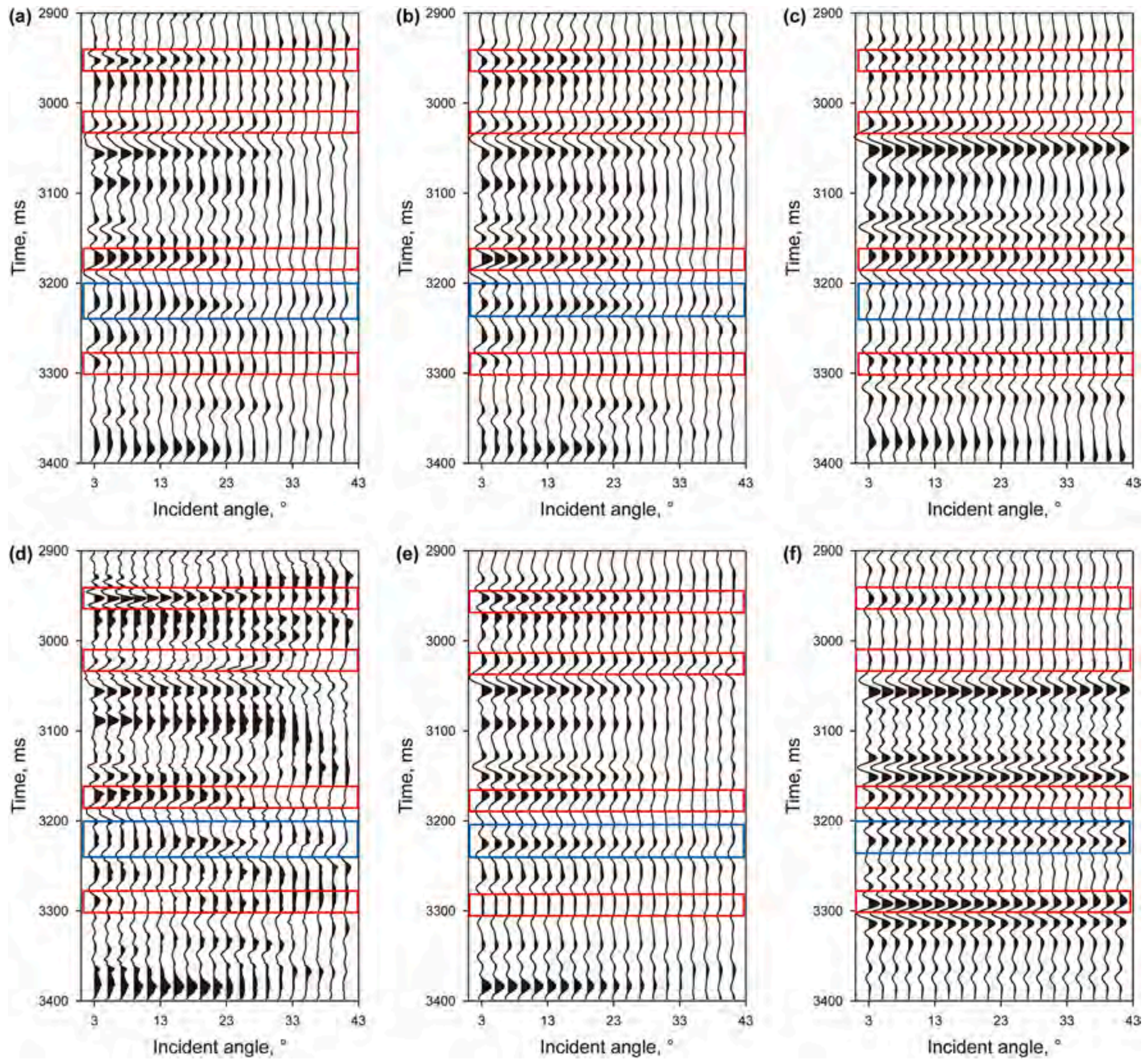

Fig. 25. The blind well validation. **(a)** The raw AVA gathers; **(b)** the high-resolution AVA gathers data obtained by deconvolution; **(c)** the high-resolution AVA gathers data obtained by pure data-driven method; **(d)** the high-resolution AVA gathers data obtained by the U-net based method; **(e)** the high-resolution AVA gathers data obtained by the proposed method; **(f)** the high-resolution AVA gathers data (0–3–50–60 Hz) obtained from the well-log data.

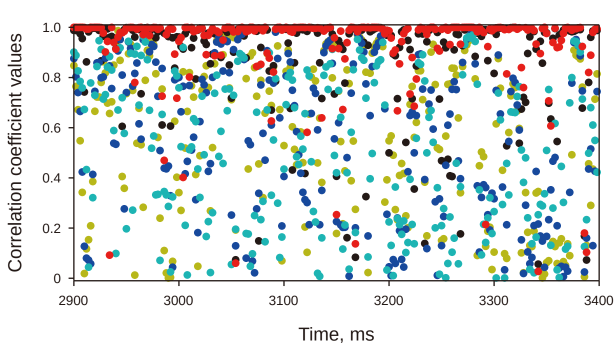

Fig. 26. Pearson correlation coefficients of AVO curves between processed data using different methods with synthetic high-frequency data from well-logs. Yellow dots denote processed seismic data by deconvolution; black dots denote processed seismic data by pure data-driven method; cyan dots denote processed seismic data by U-net based method; red dots denote processed seismic data by the proposed method.

enhancement methods consistently fail to recover the true AVO relationship. This limitation arises because these methods are typically single-trace or single-angle processing techniques, which inherently prevent the accurate restoration of the true AVO relationship during frequency enhancement.

Furthermore, our method demonstrates better generalizability compared to the purely data-driven approach. For instance, as illustrated in Fig. 14(e), where the pure data-driven method fails to preserve the true AVO relationship, our approach successfully accomplishes this. Moreover, as evidenced by other presented figures in Fig. 14, our method consistently achieves higher accuracy than the pure data-driven approach.

Fig. 15 presents the seismic traces at incident angles of 0°, 14°, and 30°, corresponding to Fig. 13, further validating the effectiveness of our approach, where the areas indicated by red arrows demonstrate that our processed seismic data achieves higher resolution and closely resembles the true high-resolution data.

4. Field data example

To validate our method, we applied it to a 160 km^2 3D survey area comprising 600 crosslines (5000–5600) and 1656 inlines (12,525–14181). Incident angles of pre-stack seismic data vary from 3° to 43° with a 2° interval. We used two training wells at (Inline 5255, Xline 13,435) and (Inline 5189, Xline 13,960), and one

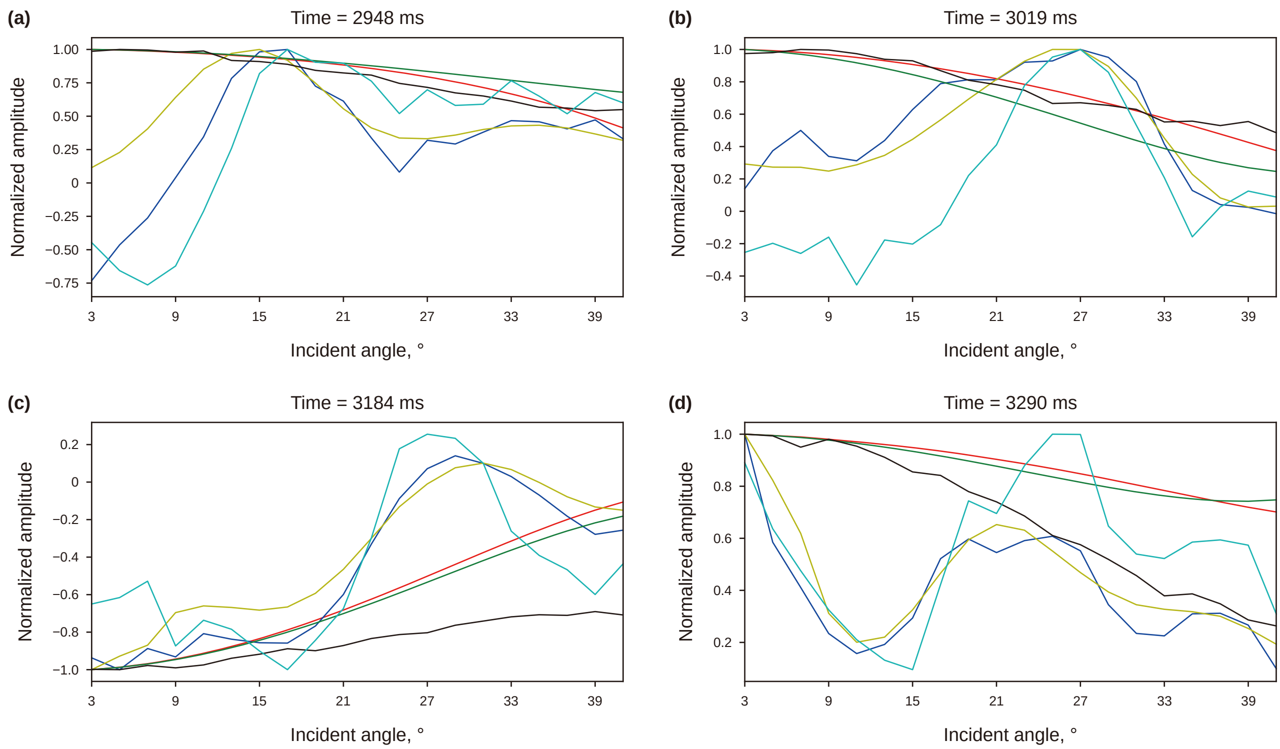

Fig. 27. AVO relationships of pre-stack seismic data at **(a)** 2948 ms, **(b)** 3019 ms, **(c)** 3184 ms, **(d)** 3290 ms. Blue lines denote raw pre-stack seismic data; green lines denote the high-resolution AVA gathers data (0–3–50–60 Hz) obtained from the well-log data; yellow lines denote processed data by deconvolution; black lines denote processed data by pure data-driven method; cyan lines denote processed data by the U-net based method; red lines denote processed data by the proposed method.

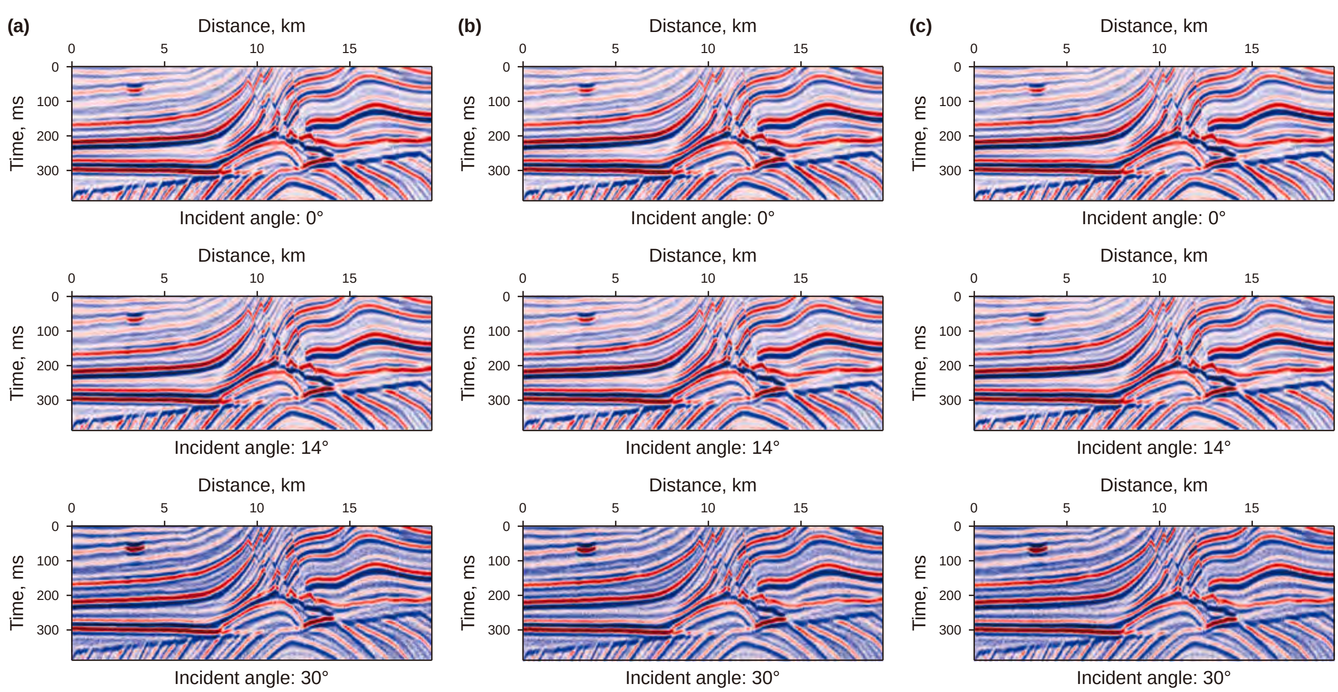

Fig. 28. Synthetic data with Gaussian noise, where **(a)** $\sigma = 0.3\sigma_0$, **(b)** $\sigma = 0.5\sigma_0$, and **(c)** $\sigma = \sigma_0$.

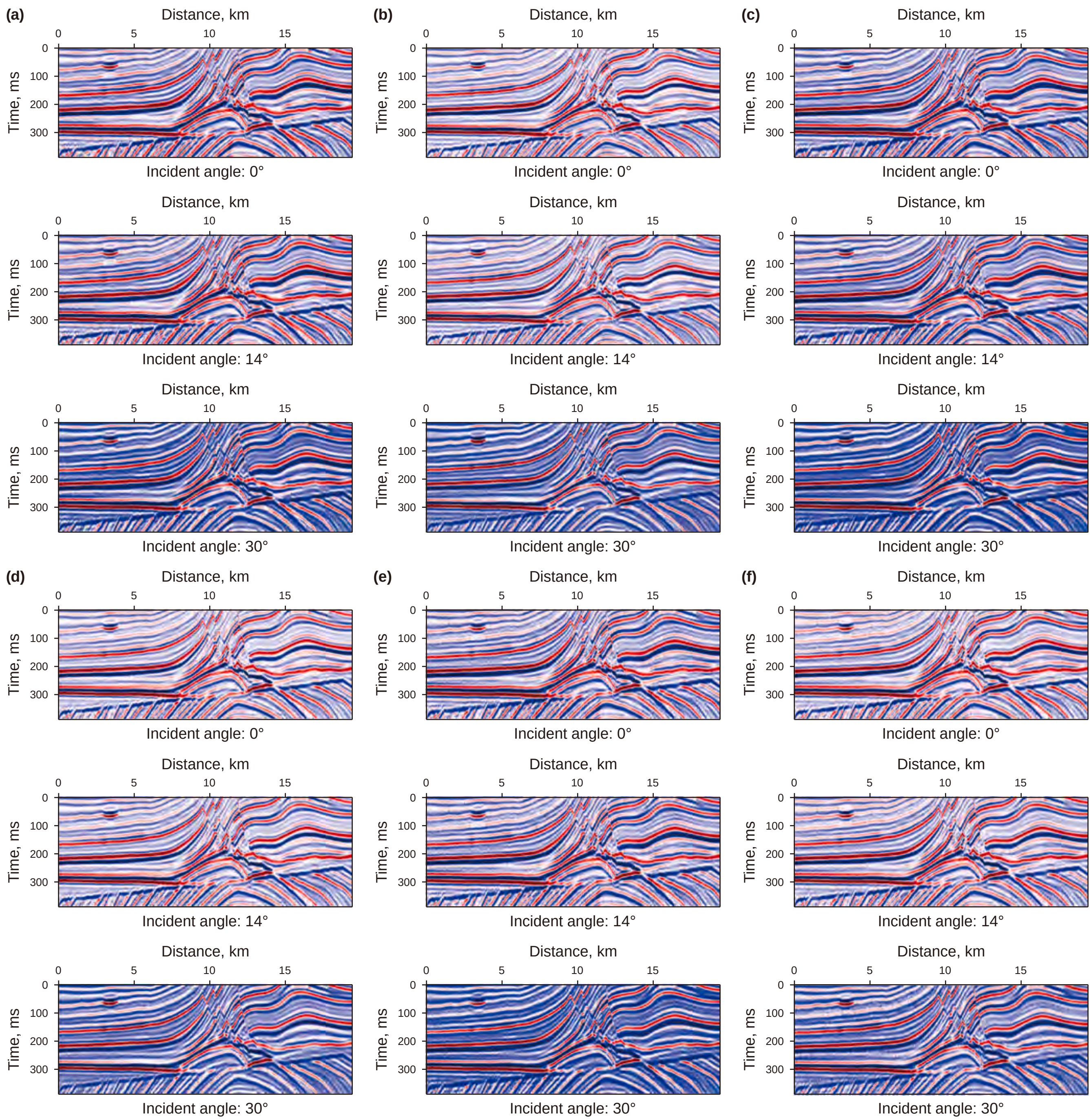

Fig. 29. The resolution-enhanced results obtained by **(a)** the deconvolution and **(b)** the proposed method applied on pre-stack seismic data contaminated with Gaussian noise ($\sigma = 0.3\sigma_0$); The resolution-enhanced results obtained by **(c)** the deconvolution and **(d)** the proposed method applied on pre-stack seismic data contaminated with Gaussian noise ($\sigma = 0.5\sigma_0$); The resolution-enhanced results obtained by **(e)** the deconvolution and **(f)** the proposed method applied on pre-stack seismic data contaminated with Gaussian noise ($\sigma = \sigma_0$).

blind-test well at (Inline 5158, Xline 13,477), marked in Fig. 16 with black triangles and pentagram, respectively. This figure also displays the 3D spatial distribution of the weight coefficient λ_r.The raw pre-stack data (main frequency: 22 Hz) are spectrally analyzed (Fig. 17) to get the wavelet used in the proposed method and establish our processing target: a broadband output of 0–3–50–60 Hz. To maintain horizontal consistency of the processed data, five consecutive AVA gathers are fed into the neural network. All other hyperparameters are configured identically to those employed in the synthetic data experiment, with the sole exception of the batch size, which is set to 512.

We use the deconvolution method, pure data-driven method, the U-net based method and our proposed method to process these field data. Table 4 presents the training and inference times for the various methods. Although our method required the longest training duration, this is considered acceptable for a 160 km^2 3D survey area. As illustrated in Fig. 18, processed by our method, the frequency band of pre-stack seismic data effectively

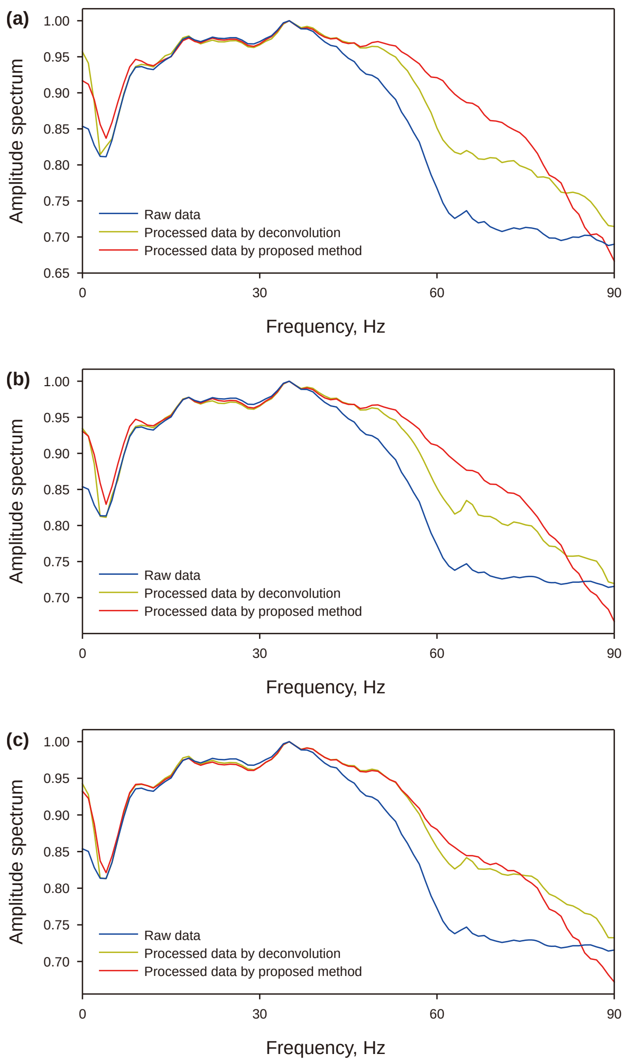

Fig. 30. Comparisons of frequency spectra of seismic data. **(a)** Pre-stack seismic data contaminated with Gaussian noise ($\sigma = 0.3\sigma_0$) and resolution-enhanced data processed by the deconvolution and the proposed method; **(b)** pre-stack seismic data contaminated with Gaussian noise ($\sigma = 0.5\sigma_0$) and resolution-enhanced data processed by the deconvolution and the proposed method; **(c)** pre-stack seismic data contaminated with Gaussian noise ($\sigma = \sigma_0$) and resolution-enhanced data processed by the deconvolution and the proposed method.

broadens to 0–3–50–60 Hz, while the frequency band of seismic data processed by deconvolution method only broadens to 0–3–35–50 Hz. The frequency bands of seismic data processed by the U-net based method and pure data-driven method are even narrow than that of raw data, this phenomenon attributed to their poor generalizability. We divided spectra into three frequency bands based on the original data's frequency range: 0–10 Hz, 10–30 Hz (the dominant frequency band of the original data), and 30–60 Hz. The ratios of the normalized amplitude spectral energy of the resolution-enhanced data to that of the original data are shown in Table 5. Our proposed method achieves energy enhancement in the low, mid, and high-frequency bands. Importantly, the high-frequency energy uplift by our method is the most pronounced when compared to other methods.

To demonstrate the effectiveness of our method further, we selected Xline 5255 and Inline 13,960 profiles to compare processed results (Figs. 19 and 20), which contain training wells, and an Xline 5158 and Inline 13,477 profiles (Figs. 21 and 22), where the test blind well is located. Comparison between processed data and raw data demonstrates that our method significantly enhances resolution across small, medium, and large incident angles, improves event continuity and maintains the improvement regardless of the presence of training wells on the seismic line. And it also can be seen from profiles that processed by U-net based method and pure data driven method have narrow frequency bands. Time slices at 2900 ms (Fig. 23) and 3100 ms (Fig. 24) demonstrate significant enhancement in both resolution and signal-to-noise ratio throughout the 3D pre-stack data processed by our proposed method and more thinner layers can be distinguished after processed by our proposed method. Fig. 25 presents the results of the blind well validation. Both our method and conventional deconvolution techniques are capable of enhancing the resolution of pre-stack seismic data, as evidenced by the blue box.

Fig. 26 shows the Pearson correlation coefficients of AVO curves between processed data using the deconvolution method and our proposed method with synthetic high-frequency data from well-log data. The deconvolution method and U-net based method cannot preserve true AVO relationships of the subsurface model across most regions, which might lead to inaccurate results in subsequent inversion processes. While pure data-driven method can preserve true AVO relationships in specific areas, it lacks generalizability, often failing to preserve accurate AVO relationships across many other regions. In contrast, our proposed method, constrained by well-log data and the Zoeppritz equation, achieves higher-resolution data that closely approximate true AVO relationships observed in the high-resolution data from the blind well. Further comparisons of the AVO relationship at different time intervals, as shown in Fig. 27, demonstrate that, compared to the other methods, our approach not only captures high-resolution detailed features but also maintains the AVO features of the pre-stack seismic data, thereby proving its effectiveness in enhancing pre-stack seismic data resolution.

5. Discussions

5.1. Noise robustness experiment

To validate robustness and test the noise tolerance of the method, we introduced three levels of Gaussian noise, respectively: Gaussian noise with $\sigma = 0.3\sigma_0$, Gaussian noise with $\sigma = 0.5\sigma_0$, and Gaussian noise with $\sigma = \sigma_0$, into the synthetic data of Marmousi2 model, where σ is the standard deviation of Gaussian noise and σ_0 is the standard deviation of the synthetic pre-stack seismic data. The noise corrupted pre-stack seismic data is shown in Fig. 28. Deconvolution and the proposed method are applied to get the high-resolution data. All other parameter settings remain consistent with the previous synthetic data experiment. As depicted in Fig. 29, both deconvolution and the proposed method can effectively enhance the resolution of the pre-stack data across a range of incident angles (0°, 14°, and 30°). Analysis of the frequency spectra of the processed seismic data (Fig. 30) reveals that both methods broaden the frequency bandwidth.

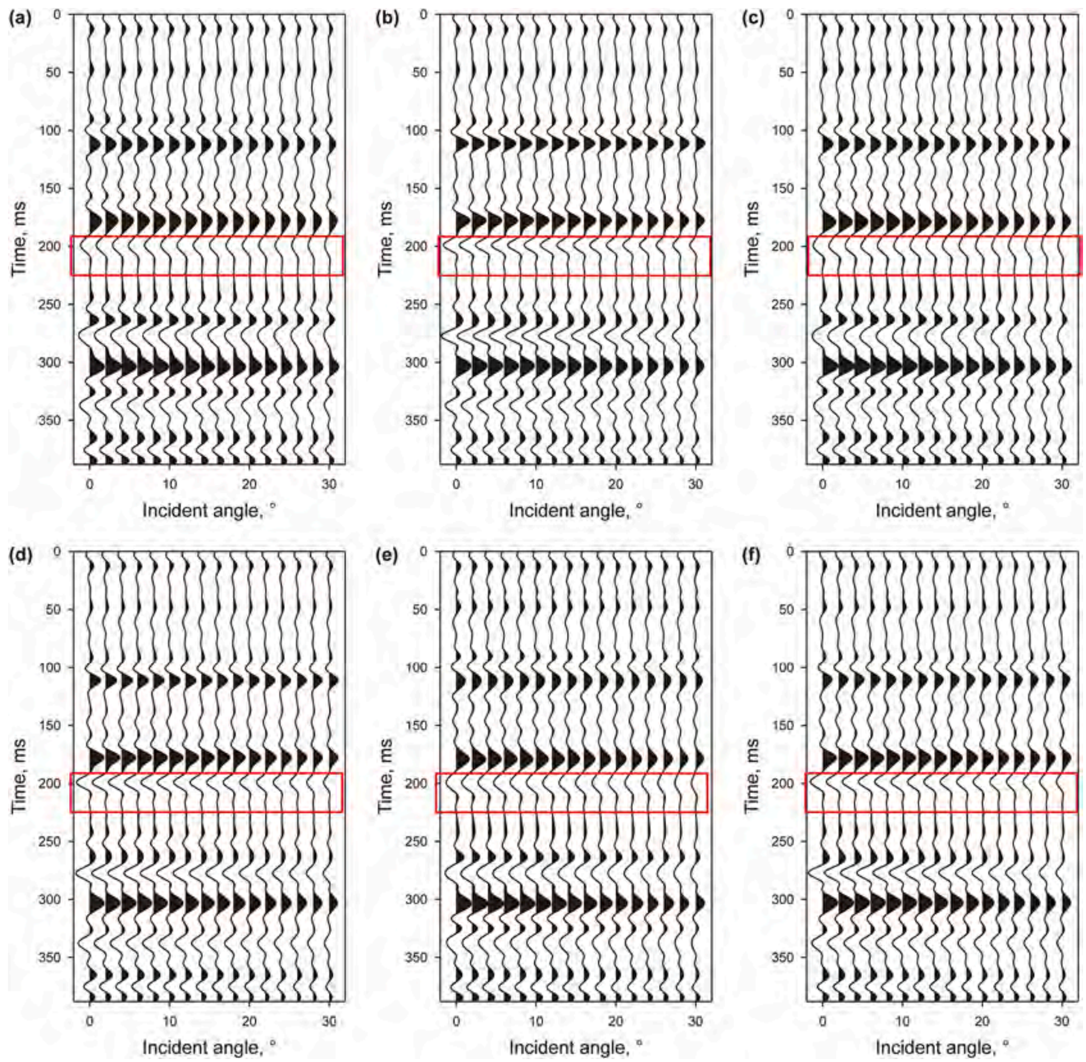

Fig. 31. AVA gathers located at 8 km processed by **(a)** the deconvolution and **(b)** the proposed method when raw pre-stack seismic data are contaminated with Gaussian noise ($\sigma = 0.3\sigma_0$); AVA gathers located at 8 km processed by **(c)** the deconvolution and **(d)** the proposed method when raw pre-stack seismic data are contaminated with Gaussian noise ($\sigma = 0.5\sigma_0$); AVA gathers located at 8 km processed by **(e)** the deconvolution and **(f)** the proposed method when raw pre-stack seismic data are contaminated with Gaussian noise ($\sigma = \sigma_0$).

However, it is also evident that the spectral broadening capability of the proposed method diminishes with increasing noise levels. Fig. 31 presents a comparison of AVA gathers, located at 8 km, processed by deconvolution and the proposed method. As highlighted by the red box in Fig. 31, the proposed method demonstrates superior resolution enhancement, even when applied to noisy data, compared to deconvolution. Furthermore, Fig. 32 illustrates the AVO relationship derived from the seismic data shown in Fig. 31 at a time of 215 ms, providing further evidence that our method better preserves the true AVO relationship during resolution enhancement. Nevertheless, it is also evident that as noise increases, the AVO relationship in the seismic data becomes increasingly difficult to discern. Therefore, for data with a low signal-to-noise ratio, our method could not preserve the true AVO relationship.

5.2. Impact of well selection

A critical aspect of our proposed method involves leveraging well data to enhance seismic data frequency while simultaneously

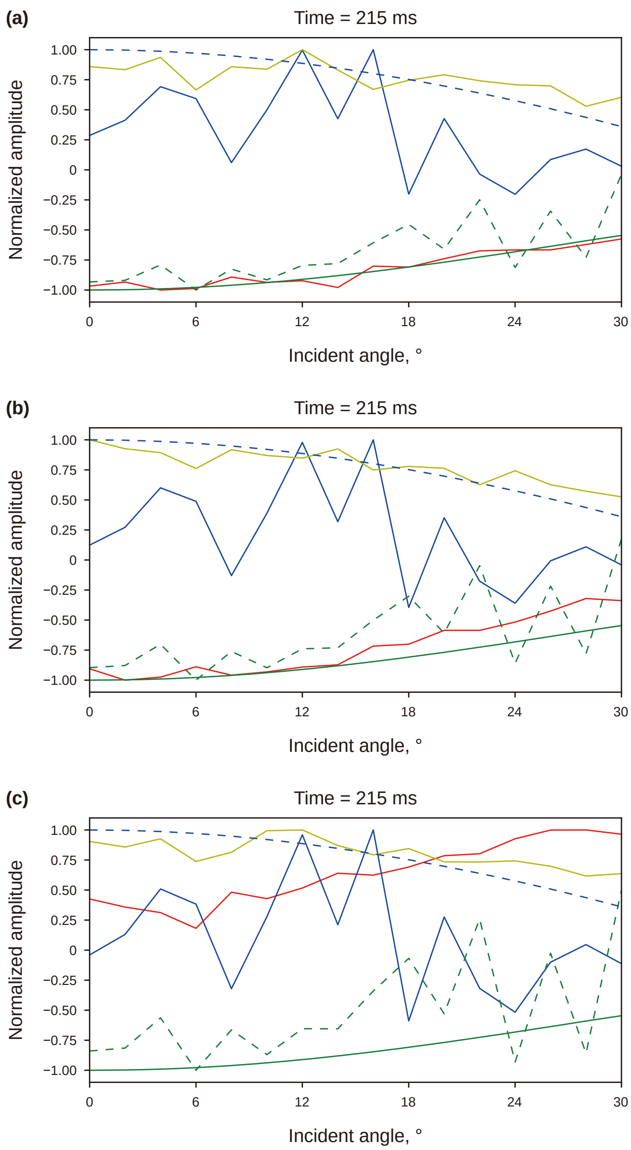

Fig. 32. Comparisons of AVO relationships between pre-stack seismic data located at 8 km contaminated with Gaussian noise at **(a)** $\sigma = 0.3\sigma_0$, **(b)** $\sigma = 0.3\sigma_0$, **(c)** $\sigma = \sigma_0$ and the corresponding resolution-enhanced results processed by deconvolution and the proposed method. Blue solid lines denote raw 0–10–40–60 Hz noise contaminated seismic data; blue dashed lines denote 0–10–40–60 Hz clean seismic data; green solid lines denote 0–3–60–90 Hz clean seismic data; green dashed lines denote 0–3–60–90 Hz noise contaminated seismic data; yellow solid lines denote processed seismic data by deconvolution; red solid lines denote processed seismic data by the proposed method.

ensuring the preservation of the true AVO relationship in the processed data. Consequently, we conducted tests to evaluate the impact of well data selection on the proposed method. In the preceding synthetic data tests, a total of four wells (A, B, C, and D) are utilized, as depicted in Fig. 5. Here, we investigate the frequency enhancement results of our method when employing only well A, wells A and D, and wells A, B, and D. All other parameter settings remain consistent with the previous synthetic data experiment.

Fig. 33 illustrates the resolution-enhanced results, showing improved resolution for pre-stack seismic data across small, medium, and large incident angles. This improvement is also corroborated by the spectral analysis presented in Fig. 34. Fig. 35 displays AVA gathers located at 3 km, 12 km, and 17 km, which are in close proximity to wells A, B, and D, respectively. In conjunction with the AVO relationship plots in Fig. 36, it can be observed that using wells A and D for resolution enhancement yields superior results compared to using only well A. Specifically, not only is the AVO relationship of seismic data at 3 km (proximal to Well D) better maintained, but also the AVO relationship at 17 km (also near Well D) is preserved with greater accuracy. Similar observations are made when employing wells A, B, and D for frequency enhancement. Theoretically, incorporating more well data leads to a more effective preservation of the AVO relationship.

6. Conclusions

We propose a semi-supervised learning method for enhancing the resolution of pre-stack seismic data using neural networks. Neural networks of our method are guided by both physical models (the convolution model and the Zoeppritz equation) and labelled datasets constructed from well-log data and corresponding AVA gathers within a semi-supervised learning framework. The labelled dataset enables the neural networks to enhance the resolution of pre-stack seismic data by leveraging well-log data and the Zoeppritz equation. Meanwhile, the physical model-driven part allows the neural networks to effectively utilize unlabeled seismic data during the training stage, improving the generalizability of the inversion process. By incorporating well-log data and the Zoeppritz equation, the proposed method ensures that the AVO relationship is preserved in the enhanced pre-stack seismic data. Experiments on 2D synthetic data and 3D field data demonstrate the effectiveness of the proposed approach. However, the method currently relies on the Zoeppritz equations, which are based on the assumption of plane wave propagation in a layered medium. As such, it is necessary to perform spherical divergence

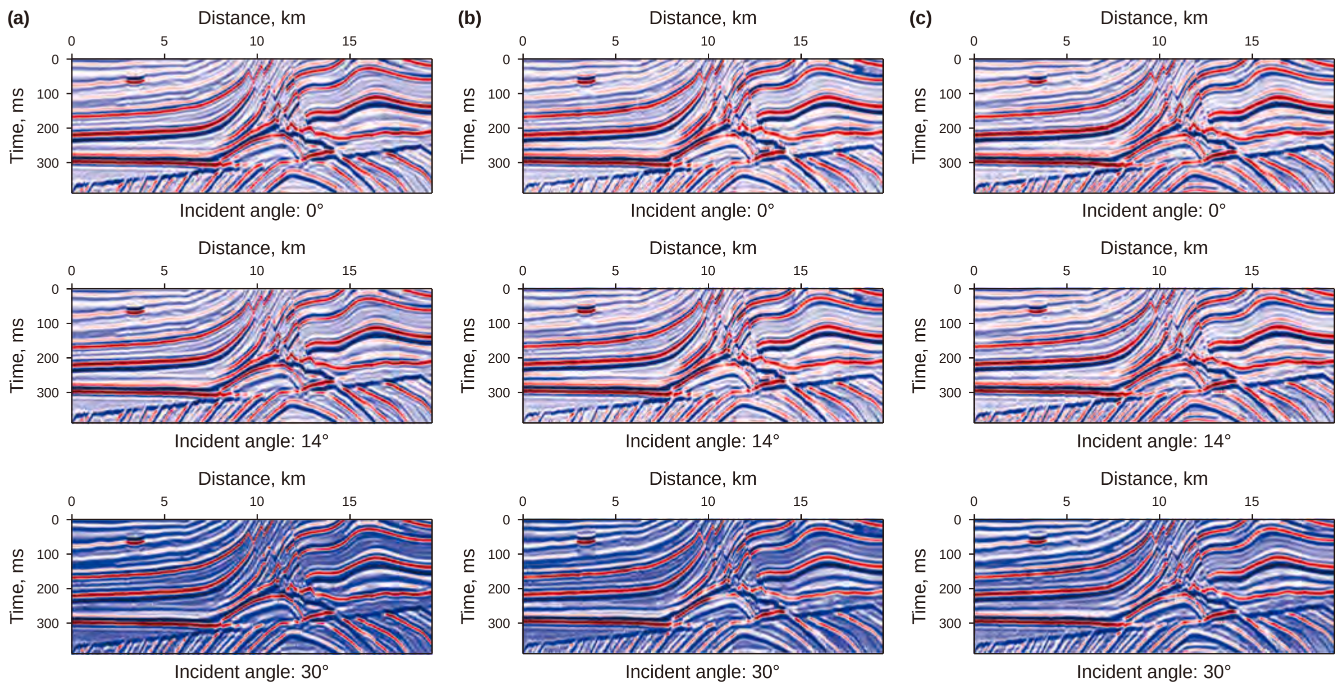

Fig. 33. Resolution-enhanced pre-stack seismic data obtained by our proposed method utilizing data from (**a**) well A, (**b**) wells A and D; (**c**) wells A, B, and D.

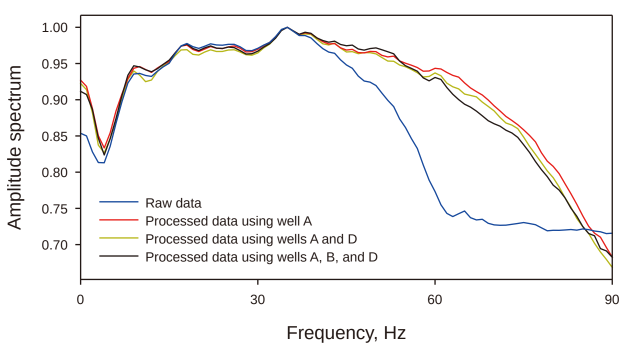

Fig. 34. Spectra of processed pre-stack seismic data utilizing data from different wells.

correction, absorption attenuation compensation, multiple wave elimination and noise suppression on the seismic data before Zoeppritz-equation-based processing. Additionally, there remains considerable room for improvement in the method's performance, particularly when applied to low signal-to-noise ratio data. Furthermore, the method does not incorporate additional prior information constraints. Future work could consider employing more accurate physical model to mitigate these restrictions, thereby embedding them into inversion frameworks capable of handling complex wavefields and extending the method's applicability to complex reservoirs.

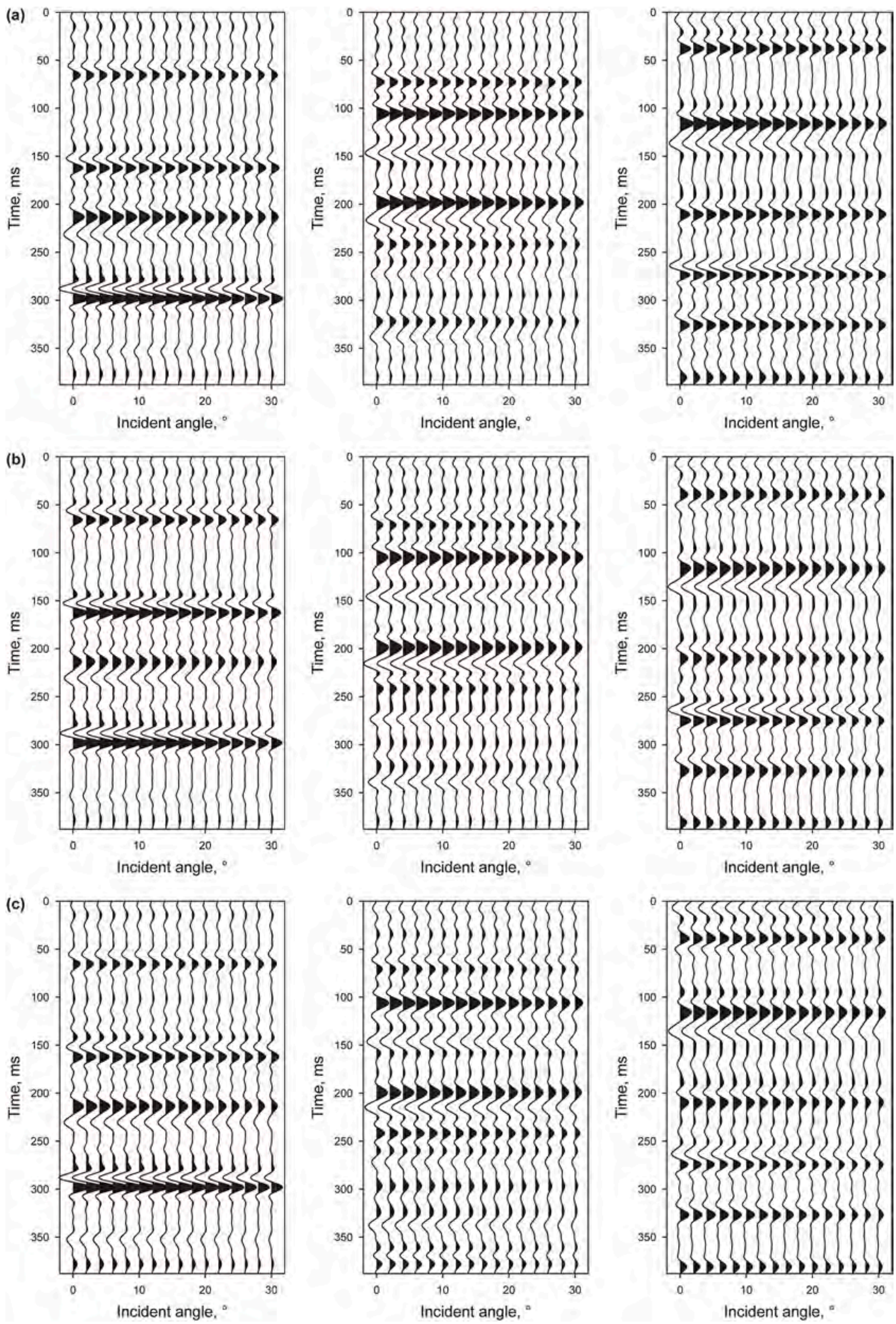

Fig. 35. AVA gathers located at 3 km (near well A), 12 km (near well B) and 17 km (near well D) processed by the proposed method utilizing data from **(a)** well A, **(b)** wells A and D; **(c)** wells A, B, and D.

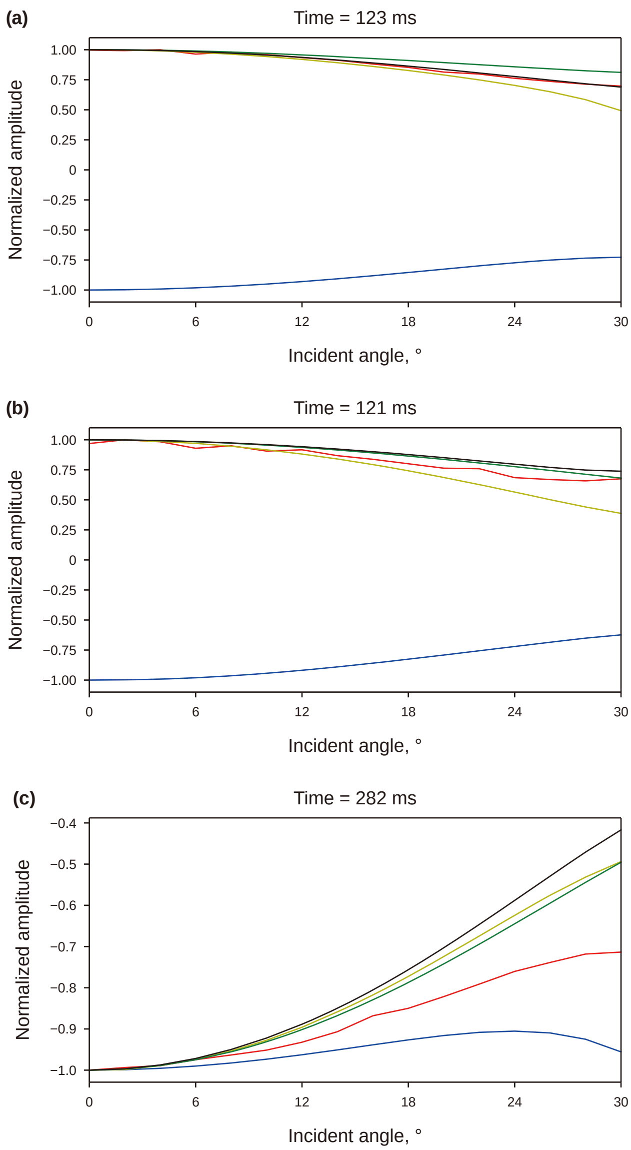

Fig. 36. AVO relationships of pre-stack seismic data located at **(a)** 3 km, **(b)** 12 km and **(c)** 17 km processed by the proposed method utilizing data from different wells. Blue lines denote raw seismic data; green lines denote true 0–3–60–90 Hz seismic data; red lines denote processed seismic data using information from well A; yellow lines denote processed seismic data using information from well A and D; black lines denote processed seismic data using information from well A, B and D.

CRediT authorship contribution statement

Shu-Liang Wu: Writing – review & editing, Writing – original draft, Methodology, Formal analysis. **Yi-Ming Jiang:** Validation, Software, Formal analysis, Data curation. **Jiang Liu:** Visualization, Software, Investigation, Data curation. **Jian Li:** Validation, Resources, Formal analysis. **De-Wen Qin:** Validation, Data curation. **Jian-Hua Geng:** Writing – review & editing, Validation, Supervision, Methodology.

Conflict of interest

We confirm that this manuscript has not been published elsewhere. All authors have approved the manuscript and agree with submission to *Petroleum Science*. We have read and have abided by the statement of ethical standards for manuscript submitted to *Petroleum Science*. The authors have no conflicts of interest to declare.

Acknowledgments

This work was supported by the National Natural Science Foundation of China (Grant No. 42330805).

References

Aki, K., Richards, P.G., 1980. Quantitative Seismology: Theory and Methods. Freeman, San Francisco, CA.
Bevc, D., Nedorub, O., Zhang, H., et al., 2019. An implementation of the seismic resolution enhancing network based on GAN. In: SEG Technical Program Expanded Abstracts, pp. 2478–2482. https://doi.org/10.1190/segam2019-3216229.1.
Castagna, J.P., Swan, H.W., Foster, D.J., 1998. Framework for AVO gradient and intercept interpretation. Geophysics 63 (3), 948–956. https://doi.org/10.1190/1.1444406.
Chen, H., Gao, J., Jiang, X., et al., 2021. Optimization-inspired deep learning high-resolution inversion for seismic data. Geophysics 86 (3), R265–R276. https://doi.org/10.1190/geo2020-0034.1.
Chen, H., Sacchi, M.D., Lari, H.H., et al., 2023. Nonstationary seismic reflectivity inversion based on prior-engaged semi-supervised deep learning method. Geophysics 88 (1), WA115–WA128. https://doi.org/10.3997/2214-4609.202011195.
Chen, S., Cao, S., Sun, Y., 2022. Enhancing the resolution of seismic data based on the nonlocal similarity. Geophys. Prospect. 70 (7), 1116–1128. https://doi.org/10.1111/1365-2478.13202.
Cheng, Q., Ma, J., Fomel, S., et al., 2022. A weakly supervised method for improving the resolution of seismic data based on cycle generative adversarial network. In: 4th International Workshop on Mathematical Geophysics: Traditional & Learning, pp. 29–32. https://doi.org/10.1190/iwmg2021-08.1.
Choi, Y., Jo, Y., Seol, S.J., et al., 2021. Deep learning spectral enhancement considering features of seismic field data. Geophysics 86 (5), V389–V408. https://doi.org/10.1190/geo2020-0017.1.
Daubechies, I., Lu, J., Wu, H.T., 2011. Synchrosqueezed wavelet transforms: An empirical mode decomposition-like tool. Appl. Comput. Harmon. Anal. 30 (5), 243–261. https://doi.org/10.1016/j.acha.2010.08.002.
Deng, J.L., 1982. Control problems of grey systems. Syst. Control Lett. 1 (5), 288–294. https://doi.org/10.1016/S0167-6911(82)80025-X.
Gao, Y., Zhang, J., Li, H., et al., 2022. Incorporating structural constraint into the machine learning high-resolution seismic reconstruction. IEEE Trans. Geosci. Rem. Sens. 60, 1–2. https://doi.org/10.1109/TGRS.2022.3157064.
Gao, Y., Zhao, D., Li, T., et al., 2023. Deep learning vertical resolution enhancement considering features of seismic data. IEEE Trans. Geosci. Rem. Sens. 61, 1–13. https://doi.org/10.1109/TGRS.2023.3234617.
Ge, Q., Cao, H., Yang, Z., et al., 2024. Deep-learning based prestack seismic inversion constrained by AVO attributes. IEEE Geosci. Rem. Sens. Lett. 21, 1–5. https://doi.org/10.1109/LGRS.2024.3373197.
Guo, A.H., Lu, P.F., Wang, D.D., et al., 2023. Improving the resolution of poststack seismic data based on UNet+ GRU deep learning method. Appl. Geophys. 20 (2), 176–185. https://doi.org/10.1007/s11770-023-1038-7.
Hale, D., 1981. An inverse Q-filter. Stanf. Explor. Proj. Rep. 26, 231–243.
Hu, C., Tu, N., Lu, W., 2013. Seismic attenuation estimation using an improved frequency shift method. IEEE Geosci. Rem. Sens. Lett. 10 (5), 1026–1030. https://doi.org/10.1109/LGRS.2012.2227933.
Huang, N.E., Shen, Z., Long, S.R., et al., 1998. The empirical mode decomposition and the Hilbert spectrum for nonlinear and non-stationary time series analysis. Proc. Roy. Soc. Lond. 454, 903–995. https://doi.org/10.1098/rspa.1998.0193.
Kim, Y., Nakata, N., 2018. Geophysical inversion versus machine learning in inverse problems. Lead. Edge 37 (12), 894–901. https://doi.org/10.1190/tle37120894.1.
Kuo, Y., Yang, T., Huang, G.W., 2008. The use of grey relational analysis in solving multiple attribute decision-making problems. Comput. Ind. Eng. 55 (1), 80–93. https://doi.org/10.1016/j.cie.2007.12.002.
Li, J., Wu, X., Hu, Z., 2022. Deep learning for simultaneous seismic image super-resolution and denoising. IEEE Trans. Geosci. Rem. Sens. 60, 1–11. https://doi.org/10.1109/TGRS.2021.3057857.
Lin, L., Zhong, Z., Cai, C., et al., 2024. SeisGAN: improving seismic image resolution and reducing random noise using a generative adversarial network. Math. Geosci. 56, 723–749. https://doi.org/10.1007/s11004-023-10103-8.
Liu, D., Niu, W., Wang, X., et al., 2023. Improving vertical resolution of vintage seismic data by a weakly supervised method based on cycle generative adversarial network. Geophysics 88 (6), V445–V458. https://doi.org/10.1190/geo2023-0006.1.
Liu, Y., Fomel, S., 2013. Seismic data analysis using local time-frequency decomposition. Geophys. Prospect. 61 (3), 516–525. https://doi.org/10.1111/j.1365-2478.2012.01062.x.
Liu, Z., Liu, D., Sacchi, M.D., et al., 2025. Physically guided high-resolution acoustic impedance inversion based on hybrid networks. IEEE Trans. Geosci. Rem. Sens. 63, 1–10. https://doi.org/10.1109/tgrs.2025.3554163.

Luo, R., Yin, Y., Chen, H., et al., 2023. Attenuation compensation and *Q* estimation of nonstationary data using semi-supervised learning. IEEE Geosci. Rem. Sens. Lett. 20, 1–5. https://doi.org/10.1109/LGRS.2023.3250610.
Robinson, E.A., 1957. Predictive decomposition of seismic traces. Geophysics 22 (4), 767–778. https://doi.org/10.1190/1.1438415.
Rutherford, S.R., Williams, R.H., 1989. Amplitude-versus-offset variations in gas sands. Geophysics 54 (6), 680–688. https://doi.org/10.1190/1.1442696.
Sacchi, M.D., 1997. Reweighting strategies in seismic deconvolution. Geophys. J. Int. 129 (3), 651–656. https://doi.org/10.1111/j.1365-246X.1997.tb04500.x.
Wang, B., Luo, R., Chen, H., 2024. Multichannel closed-loop seismic acoustic impedance estimation with nonlinear correction. IEEE Trans. Geosci. Rem. Sens. 62, 1–9. https://doi.org/10.1109/TGRS.2024.3477439.
Wang, Y., Ma, X., Zhou, H., et al., 2018. L_{1-2} minimization for exact and stable seismic attenuation compensation. Geophys. J. Int. 213 (3), 1629–1646. https://doi.org/10.1093/gji/ggy064.
Wu, S., Wang, Y., Li, Q., et al., 2024. Joint data-driven and physics-driven prestack amplitude-variation-with-angle elastic parameter inversion. Geophysics 89 (1), R17–R32. https://doi.org/10.1190/GEO2023-0135.1.
Yilmaz, Ö., 2001. Seismic Data Analysis. Society of exploration geophysicists, Tulsa. https://doi.org/10.1190/1.9781560801580.
Zhang, H.R., Liu, Y., Sun, Y.H., et al., 2024. SeisResoDiff: Seismic resolution enhancement based on a diffusion model. Pet. Sci. 21 (5), 3166–3188. https://doi.org/10.1016/j.petsci.2024.07.002.
Zhao, Y., Li, Y., Wang, S., et al., 2025. Physical model and super-resolution theory-guided unsupervised deep learning deconvolution for seismic resolution enhancement. IEEE Trans. Geosci. Rem. Sens. 63, 1–13. https://doi.org/10.1109/TGRS.2025.3531359.
Zoeppritz, K., 1919. On the reflection and propagation of seismic waves. Gottinger Nachrichten 1, 66–84.